UNIVERSIDADE FEDERAL DE MINAS GERAIS
Instituto de Geociências
Programa de Pós-Graduação em Geologia

Luiza Carneiro de Rezende

Paleoproterozoic graphitization and granitogenesis in the interior of the southern São Francisco Craton (Formiga – MG, Brazil)

224

Belo Horizonte
DATA (13/05/21)

Luiza Carneiro de Rezende

PALEOPROTEROZOIC GRAPHITIZATION AND GRANITOGENESIS IN THE INTERIOR OF THE SOUTHERN SÃO FRANCISCO CRATON (FORMIGA – MG, BRAZIL)

Versão final

Dissertação apresentada ao programa de Pós-Graduação em Geologia do Instituto de Geociências da Universidade Federal de Minas Gerais como requisito para obtenção do título de Mestra em Geologia Regional.

Orientador: Prof. Dr. Alexandre de Oliveira Chaves

BELO HORIZONTE
2021

R467p 2021

Rezende, Luiza Carneiro de.
Paleoproterozoic graphitization and granitogenesis in the interior of the southern São Francisco Craton (Formiga - MG, Brazil) [manuscrito] / Luiza Carneiro de Rezende. – 2021.
51 f., enc.: il. (principalmente color.)

Orientador: Alexandre de Oliveira Chaves.
Dissertação (mestrado) – Universidade Federal de Minas Gerais, Instituto de Geociências, 2021.
Área de concentração: Geologia Regional.
Inclui bibliografia.

1. Petrologia – Minas Gerais – Teses. 2. Geoquímica – Minas Gerais – Teses. 3. Raman, Espectroscopia de. – Teses. 4. Tempo geológico – Teses. I. Chaves, Alexandre de Oliveira. II. Universidade Federal de Minas Gerais. Instituto de Geociências. III. Título.

CDU: 552(815.1)

Ficha catalográfica elaborada por Graciane Aparecida de Paula – CRB6 3404

UNIVERSIDADE FEDERAL DE MINAS GERAIS

PROGRAMA DE PÓS-GRADUAÇÃO EM GEOLOGIA

FOLHA DE APROVAÇÃO

Paleoproterozoic graphitization and granitogenesis in the interior of the southern São Francisco Craton (Formiga – MG, Brazil)

LUIZA CARNEIRO DE REZENDE

Dissertação submetida à Banca Examinadora designada pelo Colegiado do Programa de Pós-Graduação em GEOLOGIA, como requisito para obtenção do grau de Mestre em GEOLOGIA, área de concentração GEOLOGIA REGIONAL.

Aprovada em 13 de maio de 2021, pela banca constituída pelos membros:

Prof. Alexandre de Oliveira Chaves - Orientador
UFMG

Prof. Daniel Andrade Miranda
UFES

Prof. Adolf Heinrich Horn
UFMG

Belo Horizonte, 13 de maio de 2021.

AGRADECIMENTOS

De todos os desafios que envolvem a conclusão de uma pesquisa de mestrado, enfrentar uma pandemia com certeza não é algo que eu esperava. Além das dificuldades para acessar laboratórios, o medo do vírus e a ansiedade causada pelo isolamento social com certeza foram grandes obstáculos que tive que enfrentar neste processo. Mas felizmente não passei por este período sozinha.

Agradeço aos meus pais e meu irmão, que sempre apoiaram minha jornada pelo caminho das pedras na geologia e na carreira acadêmica e estiveram comigo também fisicamente durante este período tão conturbado.

Aos amigos da geologia, de todos os lugares do Brasil, meu muito obrigada. Pelos momentos de descontração e por me ensinarem tanto, muito além do que a universidade é capaz de proporcionar. Em especial ao Calops, meu parceiro de vida.

Às amigas do Ensino Médio e da vida, agradeço por sempre estarem comigo, entenderem minhas ausências, devido aos trabalhos de campo e congressos, e apoiarem incondicionalmente todos os meus sonhos.

Gostaria de agradecer e enaltecer todas as mulheres geocientistas que enfrentam comigo todos os desafios de cursar e seguir carreira em uma área ainda tão machista e patriarcal. Não é fácil, mas juntas estamos mudando esta realidade, rumo a um futuro com mais oportunidades e equidade. Vocês me dão força todos os dias.

Ao professor Alexandre de Oliveira Chaves, pela orientação, paciência e ensinamentos.

Este trabalho foi realizado no âmbito do Programa de Pós-graduação em Geologia do Instituto de Geociências da Universidade Federal de Minas Gerais (PPG Geologia – IGC/UFMG), com apoio da Pró-Reitoria de Pós-Graduação (PRPG) da UFMG e da Coordenação de Aperfeiçoamento de Pessoal de Nível Superior – Brasil (CAPES) – Código de Financiamento 001.

A todos aqueles que estiveram envolvidos direta e indiretamente na minha trajetória rumo a realização do meu sonho de ser professora: minha eterna gratidão.

“A educação é um ato de amor, por isso, um ato de coragem. Não pode temer o debate. A análise da realidade. Não pode fugir à discussão criadora, sob pena de ser uma farsa.”

- Paulo Freire

RESUMO

Os crátons brasileiros vivenciaram, durante a era Paleoproterozóica, eventos orogênicos que modificaram os embasamentos arqueanos e as sequências sedimentares. Durante a transição entre os períodos Riaciano para Orosiriano, ocorreu no Cráton do São Francisco Meridional uma colisão entre os complexos metamórficos arqueanos Divinópolis e Campo Belo, relacionada ao fechamento de uma bacia oceânica, seguida do colapso do orogênico. Um grande evento magmático intraplaca, que é representado na área pelo enxame de diques Pará de Minas, ocorreu durante o início do período Estateriano. Nas proximidades dos municípios de Formiga e Itapecerica (Minas Gerais - Brasil) são registradas ocorrências de xisto grafitoso entre os complexos citados. Além disso, ocorrem metagranitos peraluminosos ao redor de paragnaisses kondalíticos e formações ferríferas bandadas de alto grau metamórfico. Para compreender a origem e o metamorfismo da grafita, foram realizados estudos petrográficos, análises de difração de raio-X (DRX) e espectroscopia Raman. Os metagranitos foram estudados com base em análises petrográficas, geoquímicas e geocronológicas de U-Th-Pb em monazita. Os métodos DRX e Raman revelaram que as temperaturas registradas pela grafita giram em torno de 460°C. No entanto, dados Raman mostraram que os tamanhos do cristalito correspondem a condições de maior grau metamórfico (fácies anfibolito a granulito). Temperaturas de 460°C estão provavelmente associadas a processos hidrotermais sofridos pela grafita ao longo de falhas no estágio pós-colisional. A presença de todorokita, um mineral típico de nódulos de Mn do fundo do mar formado por microrganismos, em associação com a grafita, sugere uma origem biogênica para a ocorrência da grafita. O metagranito foi caracterizado como metamonzogranito peraluminoso do tipo S (origem metassedimentar), com assinatura geoquímica crustal e gênese relacionada à anatexia em ambiente sin- a pós-colisional. Os resultados geocronológicos produziram idades Orosiriana (~ 1,90 Ga) e Estatheriana (~ 1,78 Ga) para os metagranitos. Esses resultados estão relacionados, respectivamente, ao colapso do orógeno Riaciano-Orosiriano e ao aquecimento regional, associado à província ígnea gigante Avanavero-Xiong'er que é representada na área pelo enxame de diques Pará de Minas.

Palavras-chave: Grafita. Espectroscopia Raman. Difração de raio-X. Granito. Paleoproterozoico. Monazita. Geoquímica. Craton São Francisco.

ABSTRACT

The Brazilian cratons experienced, during the Paleoproterozoic Era, orogenic events that modified the Archean basement and sedimentary successions. During the transition of Rhyacian to Orosirian periods, in the southern São Francisco Craton, a collision between the Archean Divinópolis and Campo Belo metamorphic complexes, related to the closure of an oceanic basin, occurred followed by the collapse of the orogen. A huge intraplate magmatic event, that is represented in the area by the Para de Minas dyke swarm, occurred during the beginning of the Statherian period. In the vicinity of the cities of Formiga and Itapecerica (Minas Gerais – Brazil) occurrences of graphite schist are reported between the complexes aforementioned. Furthermore, peraluminous metagranite occurs surrounding high metamorphic grade khondalitic paragneisses and banded iron formations. To comprehend origin and metamorphism of the graphite, petrographic studies, X-ray diffraction (XRD) and Raman spectroscopy analyses have been done. The metagranites were studied based on petrographic, geochemical, and monazite U-Th-Pb geochronological analyses. XRD and Raman methods revealed that the temperatures recorded by graphite are around 460°C. However, Raman data showed that the crystallite sizes correspond to higher metamorphic grade conditions (amphibolite to granulite facies). Temperatures of 460°C are probably associated with hydrothermal processes disturbing graphite along faults in post-collisional stage. The presence of todorokite, a mineral typical of deep-sea Mn nodules formed by microorganisms, in association with graphite from Formiga, suggests a biogenic origin for the graphite occurrence. The metagranite was characterized as S-type (metasedimentary origin) peraluminous metamonzogranites, with crustal geochemical signature, and genesis related to anatexis in syn- to post-colisional environment. The geochronological results yelded Orosirian (~1,90 Ga) and Statherian (~1,78 Ga) ages for metagranites. These results are related, respectively, to the collapse of the Rhyacian-Orosirian orogen and to the regional warming, associated with the Avanavero-Xiong'er large igneous province that is represented in the area by the Pará de Minas dykes swarm.

Keywords: Graphite. Raman spectroscopy. X-ray diffraction. Granite. Paleoproterozoic. Monazite. Geochemistry. São Francisco Craton.

SUMMARY

INTRODUCTION

The São Francisco Craton (SFC) is a tectonic domain (Almeida, 1977) (Fig. 1B) surrounded by Neoproterozoic orogens. Its southern portion has been object of investigation due to the presence of rocks of economic interest and the complex tectonic history. This dissertation characterizes graphite schists and metagranites that occur in the southern SFC in order to comprehend the Paleoproterozoic evolution of Formiga region (Fig. 1C).

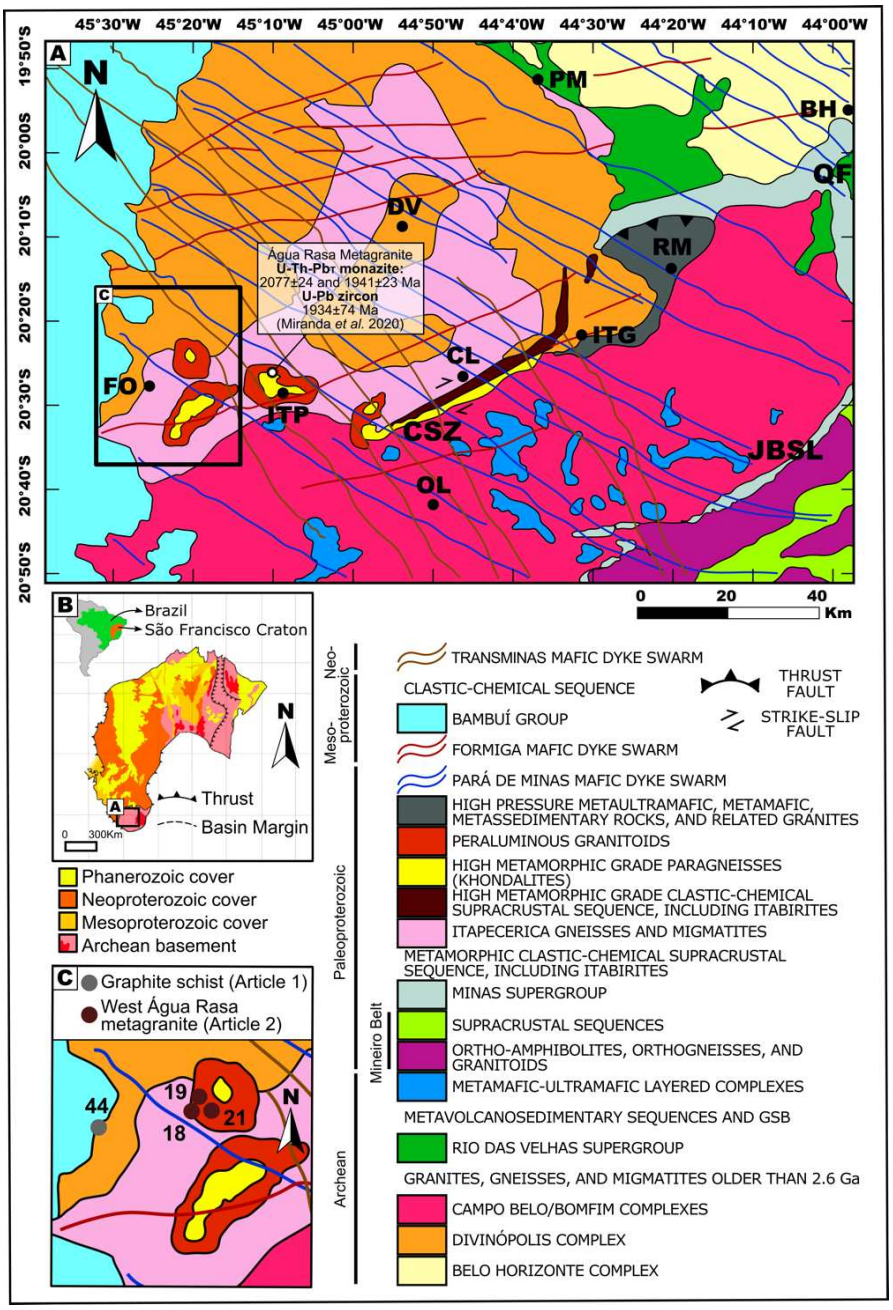

Fig. 1 (A) Geological map of the Southern São Francisco Craton interpreted from geophysics, with the area of study highlighted. CSZ – Cláudio Shear Zone, JBSL – Jeceaba-Bom Sucesso Lineament, QF – Quadrilátero Ferrífero, Cities: BH – Belo Horizonte, CL – Cláudio, DV – Divinópolis, FO – Formiga, ITG – Itaguara, ITP – Itapecerica, OL – Oliveira, PM – Pará de Minas, RM – Rio Manso. Modified after Chaves and porcher (2020). (B) São Francisco Craton simplified map, with its Southern region highlighted. Modified after Drummond et al. (2015). (C) Detailed area of study with sample collection spots.

The southern São Francisco Craton (SFC) (Fig. 1A) is formed by an Archean crust (3.5 – 2.6 Ga), Paleoproterozoic rocks, and Neoproterozoic clastic-chemical sediments. The basement is formed by granite-gneisses rocks (Farina et al. 2015; Teixeira et al. 2017) and greenstone belts from Rio das Velhas Supergroup, which comprises mafic-ultramafic rocks, intermediate-felsic volcanic and volcanoclastic rocks sediments (Dorr, 1969; Baltazar and Zucchetti, 2007). The Paleoproterozoic cover is composed of clastic-chemical metasedimentary rocks, including the banded iron formations from Minas Supergroup. The Neoproterozoic cover consists of pelitic-carbonate sedimentary rocks from Bambuí Group (Teixeira et al. 2017).

The basement of southern SFC (Fig. 1A) is represented by Campo Belo, Divinópolis, Bonfim and Belo Horizonte metamorphic complexes (Machado Filho et al., 1983; Teixeira et al., 1996). The supracrustal sequence is composed of Paleoproterozoic clastic-chemical metasedimentary rocks, with minimum deposition around 2.0 Ga, and also the typical banded iron formations from the Quadrilátero Ferrífero (Machado et al., 1996; Moreira et al., 2016). Above occur the Neoproterozoic pelitic-carbonate sedimentary rocks from Bambuí Group (Alkmim and Martins-Neto, 2001). Occurrences of graphite with biogenic origin (Miranda et al. 2019) are reported in southern SFC, where Itapecerica Supracrustal Sequence has been described (Campello et al. 2015; Chaves et al. 2015; Teixeira et al. 2017). Finally, all the southern SFC is crosscuted by mafic dykes (Chaves, 2013) that had important influence in rocks studied in this dissertation.

A Rhyacian-Orosirian accretionary orogeny resulted in extensive reworking of the margins of the southern portion of the SFC (Noce et al., 2007) and is responsible for the formation of the Mineiro Belt (Noce et al., 1998; Ávila et al., 2014; Teixeira et al., 2015) also shown in figure 1A. Based on chemical ages found in monazites in sillimanite-cordierite-garnet-biotite gneiss (graphite-rich khondalitic rocks), Chaves et al. (2015) were the first to suggest the occurrence of a Paleoproterozoic event in the Itapecerica region, which was confirmed by isotopic ages from zircons of 2.05-2.03 Ga (U-Pb) found by Carvalho et al. (2017) in the interior of the basement.

From the data generated by the Aerogeophysical Survey Program of the Government of Minas Gerais/CODEMIG, whose survey and report were carried out by the company Lasa (2001), three elliptical and synform anomalies can be seen by gamma-spectrometric data (Fig. 2). These ellipses are structured as follows: the inner portions correspond to the supracrustal sequence conditioned by shear zones of preferential directions E-W and NE-SW, while the outer part corresponds to the peraluminous metagranitoid, that are named as Água Rasa

Metagranite (Miranda et al. 2020). These structures were also indicated by Ruy et al. (2006) and Zacchi et al. (2007).

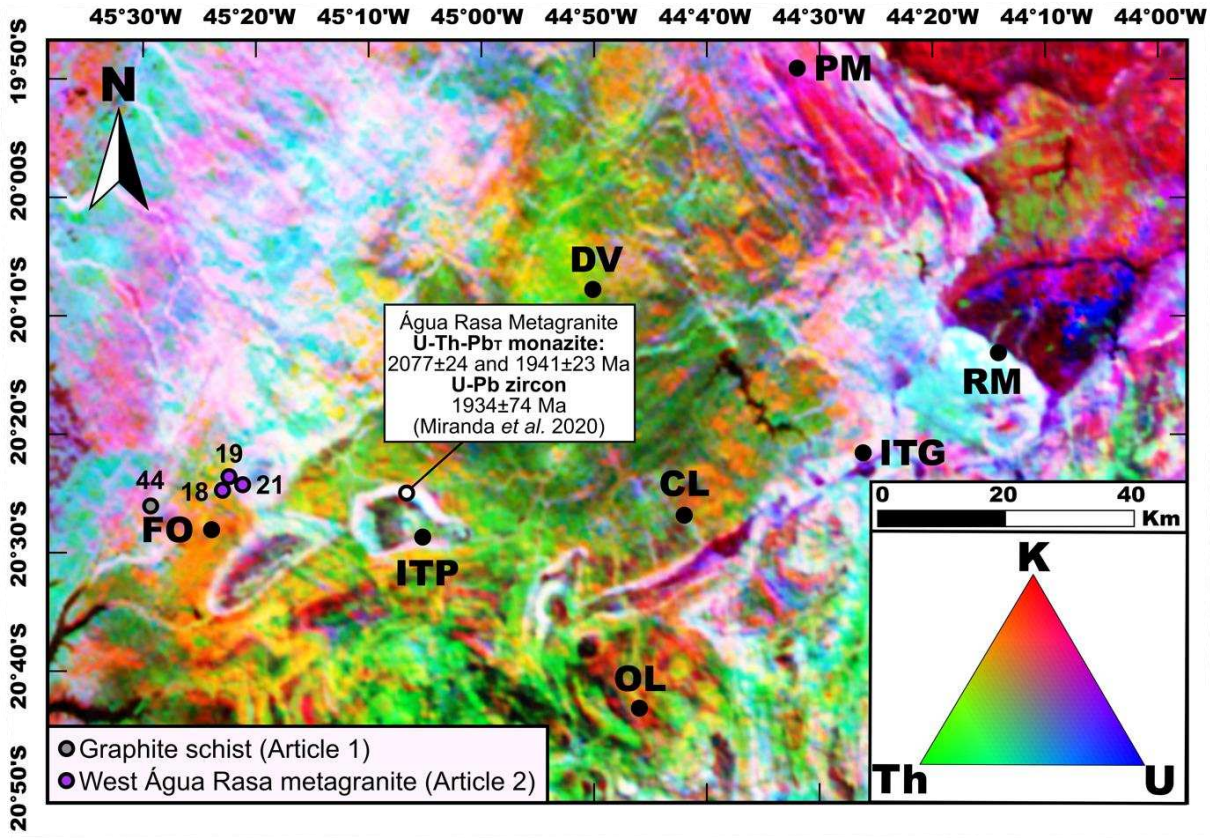

Fig. 2 - K-Th-U ternary gamma spectrometric image of the region of study with the samples collecting sites highlighted (CPRM-CODEMIG, 2014). Cities: BH – Belo Horizonte, CL – Cláudio, DV – Divinópolis, FO – Formiga, ITG – Itaguara, ITP – Itapecerica, OL – Oliveira, PM – Pará de Minas, RM – Rio Manso.

The aim of this study to contribute to the understanding of the Paleoproterozoic tectonic evolution of the southern São Francisco Craton. To achieve this objective, graphite schist and metagranite samples were characterized in order to correlate to events discussed in this area. The samples were collected in the region between the cities of Formiga and Itapecerica (MG – Brazil) (Fig. 1C and Fig. ***2***) and were studied in two scientific articles presented next.

The first paper - ***Origin and metamorphism of graphite from Formiga – MG (Brazil)*** - is published in the Brazilian Journal of Geology with DOI: https://doi.org/10.1590/2317-4889202120200083 and the second - ***Petrology, geochemistry and monazite U-Th-Pb ages of West Água Rasa metagranites from Southern São Francisco Craton – Brazil*** – not yet published until the date of the defense.

Both articles, in accordance with the requirements of the respective scientific journals, have formatting, numbering of items and independent figures, and they do not follow the general order of this volume.

The first article characterizes the origin, crystallinity, and metamorphism temperature of graphite using XRD and Raman spectroscopy. The results are compared to previous studies to corroborate to the understanding of the tectonic model proposed for the Rhyacian-Orosirian orogeny in the southern São Francisco Craton.

The second paper characterizes the nature, origin, and age of what was called West Água Rasa metagranite, using petrography, geochemistry, and monazite U-Th-Pb geochronology. The results are also used to corroborate to the understanding of the Paleoproterozoic tectonic context in the southern SFC.

ARTICLE I – Origin and metamorphism of graphite from Formiga – MG (Brazil)

Authors: Luiza Carneiro de Rezende[a], Alexandre de Oliveira Chaves[a], Sérgio Luis Lima de Moraes Ramos[b].

[a] Geology Department – Institute of Geosciences – Federal University of Minas Gerais (IGC - UFMG). Av. Antônio Carlos, 6627, Belo Horizonte – MG, CEP 31270-901.

[b] Technological Center of Nanomaterials – Federal University of Minas Gerais (CTnano - UFMG). Rua Professor José Vieira de Mendonça, nº 520 - Engenho Nogueira, Belo Horizonte – MG (Brazil), 31310-260.

Published in periodic Brazilian Journal of Geology.

DOI: https://doi.org/10.1590/2317-4889202120200083

ABSTRACT

During the Paleoproterozoic Era, the Brazilian cratons experienced orogenic events that modified the Archean basement and sedimentary successions. In the southern São Francisco Craton, it can be recognized evidence of an orogenic event that happened between Rhyacian and Orosirian periods. It is related to the closure of an oceanic basin at this time, which led to the collision between the Archean Divinópolis and Campo Belo metamorphic complexes. Graphite schist occurs close to the cities of Formiga and Itapecerica (Minas Gerais), located between these complexes. To contribute to the understanding of the origin and metamorphism of the graphite from Formiga, petrographic studies, X-ray diffraction (XRD) and Raman spectroscopy analyses have been done. XRD and Raman methods revealed that the temperatures recorded by graphite are around 460°C. However, Raman data showed that the crystallite sizes correspond to higher metamorphic grade conditions (amphibolite to granulite facies). Temperatures of 460°C are probably associated with hydrothermal processes along faults in post-collisional stage. The presence of todorokite, a mineral typical of deep-sea Mn nodules formed by microorganisms, in association with graphite from Formiga, suggests a biogenic origin for the graphite occurrence.

KEYWORDS: Southern São Francisco Craton, Raman Spectroscopy, X-ray Diffraction, graphite

1. INTRODUCTION

Graphite and diamond are the polymorph occurrence of native carbon on the nature (Harlow 1998). Graphite has a growing economic value due to its modern technological use as graphene source (Simandl et al. 2015). Formed in several geological settings, graphite is most commonly found in metamorphic rocks, especially in orogenic belts. Graphite can be formed

through maturation and metamorphism of biogenic carbonaceous material (CM); as precipitation from C-O-H fluids; mantle-derived; and through reduction of carbonates (Simandl et al. 2015).

There is a vast combination of variables like temperature, pressure, kinetics, composition of country rocks and presence or absence of fluids that can influence the formation of this mineral (Wintsch et al. 1981, Luque et al. 1998, Galvez et al. 2013). The graphite formed by biogenic CM undergoes a progressive and irreversible process called graphitization (Buseck and Beyssac 2014). It occurs in temperature and pressure of burial metamorphism, and decreases the hydrogen-to-carbon (H/C) and oxygen-to-carbon (O/C) ratios, transforming disordered and non-crystalline CM in crystalline graphite (Kwiecińska and Petersen 2004) (Fig. 1). The process of graphitization does not depend on the metamorphic pressure, although it is influenced by the oxygen fugacity and metamorphic temperature (Tagiri and Oba 1986). There are two forms to quantify the metamorphic temperature associated to the graphitization of biogenic CM:

- by Raman spectroscopy geothermometry, from low (~330°C) to high-grade metamorphism (~600°C) (Beyssac et al. 2002);
- by X-ray diffraction (XRD) geothermometry, for metamorphism above 600°C (Wada et al. 1994).

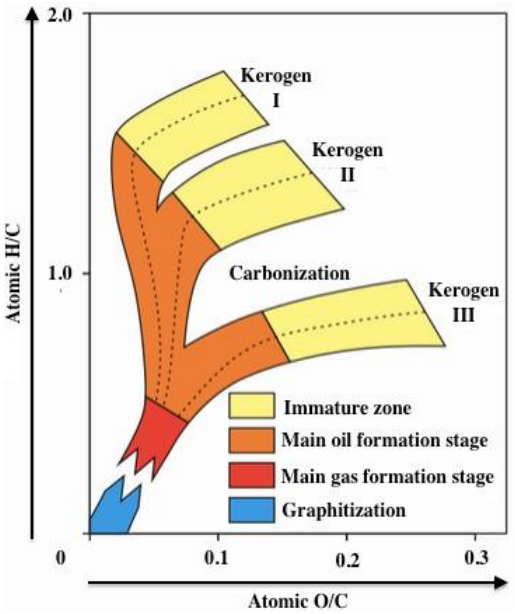

Fig. 1. Kerogen maturation in terms of H/C and O/C atomic ratios. Modified from Buseck and Beyssac (2014).

An efficient method to analyse the origin of CM is to evaluate its isotopic composition, inasmuch as Buseck and Beyssac (2014) indicate that this kind of deposit preserves the $\delta^{13}C$ between -35 and -20‰ biologic signature. A variety of minerals can be formed in this

condition, as is the case of todorokite ((Mn, Mg, Ca, Ba, Na, K)$_2$ $Mn_5O_{12}.3H_2O$), which is formed by the accumulation of Mn-oxides (Lowenstam 1981), and can be used as evidence of biogenic activity on seafloor (Burns et al. 1983).

Graphite schist occurs at southern São Francisco Craton, in the Itapecerica Supracrustal Sequence, associated with the collision between the Archean Divinópolis and Campo Belo metamorphic complexes. In Itapecerica (Minas Gerais (MG), Brazil), Miranda et al. (2019) characterized two different forms of graphite. They presented $\delta^{13}C$ between -21.23 and -27.89‰, indicating biogenic source, and high-grade metamorphism associated with a syn-collisional stage, with average temperature around 729°C (metamorphic graphite), and hydrothermalism associated with post-collisional stage, around 611°C (recrystallized graphite).

In order to complement the study of Miranda et al. (2019), this paper aims to characterize the origin, crystallinity and metamorphism temperature of graphite from an area near the city of Formiga (MG), a city located about 40 km west of Itapecerica (MG) (Fig. 2), using XRD and Raman spectroscopy. The results are compared to previous studies to corroborate to the understanding of the tectonic model proposed for the Rhyacian-Orosirian orogeny in the southern São Francisco Craton.

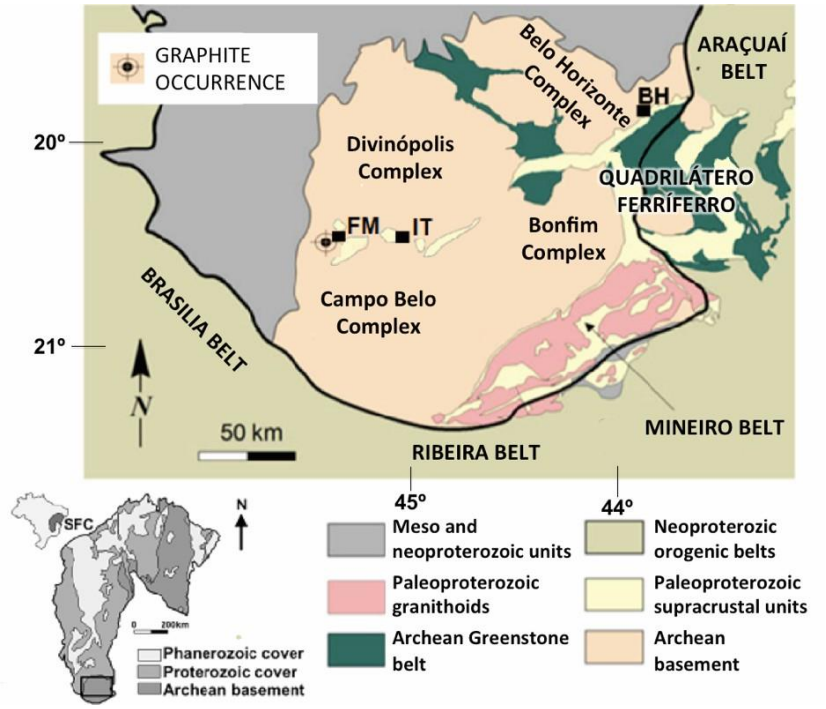

Fig. 2. Geology of meridional sector of São Francisco Craton (SFC). BH – Belo Horizonte. FM – Formiga. IT – Itapecerica (modified from Alkmim and Teixeira, 2017).

2. GEOLOGICAL SETTING

The São Francisco Craton (SFC) is a tectonic domain (Almeida 1977) (Fig. 2) surrounded by Neoproterozoic orogens. Its southern sector is composed by Archean crust, with age between 3.5 and 2.6 Ga, that is formed mostly by granite-gneisses rocks (Farina et al. 2015) and greenstone belts (Rio das Velhas Supergroup) constituted by mafic-ultramafic, intermediate-felsic volcanic and volcanoclastic rocks (Noce et al. 1998) with terrigenous sediments (Dorr 1969, Baltazar and Zucchetti 2007).

The basement comprises the Campo Belo, Divinópolis, Bonfim and Belo Horizonte metamorphic complexes (Fig. 2) (Machado Filho et al. 1983, Teixeira et al. 1996). The supracrustal sequence is formed by the Minas Supergroup, which is characterized by clastic-chemical metasedimentary rocks from the Paleoproterozoic (minimum deposition around 2.0 Ga), including the banded iron formations of the Quadrilátero Ferrífero (Machado et al. 1996, Moreira et al. 2016), and also the Bambuí Group, formed by pelitic-carbonate sedimentary rocks with Neoproterozoic age (Alkmim and Martins-Neto 2001).

The Mineiro Belt (Noce et al. 1998, Ávila et al. 2014, Teixeira et al. 2015) was formed by accretionary orogeny and occurred between Rhyacian and Orosirian, which resulted in extensive reworking of regions placed at the margins of the southern SFC (Noce et al. 2007). Chaves et al. (2015) suggested the existence of a Paleoproterozoic event in the Itapecerica region based on chemical ages found in monazites in sillimanite-cordierite-garnet-biotite gneiss (graphite-rich khondalitic rocks), which was confirmed by Carvalho et al. (2017), that found isotopic ages from zircons of 2.05–2.03 Ga (U-Pb) in the interior of the basement.

Occurrences of graphite with $\delta^{13}C$ between -21.23 and -27.89‰, indicating biogenic origin, (Miranda et al. 2019) are reported in this area, where Itapecerica Supracrustal Sequence has been described (Campello et al. 2015, Chaves et al. 2015, Teixeira et al. 2017). The studied area is located near the city of Formiga, where the graphite schist occurs between the Divinópolis and Campo Belo complexes (Fig. 2).

3. METHODS AND RESULTS

Three samples were collected at the Formiga area (20º26’40.4”S, 40º30’04.3”W). Samples LR44A and LR44C were chipped from an abandoned trench (Fig. 3A) and sample LR44B was chipped about 5 m away. Both collection spots are formed by fine grained graphite schist composed of quartz, graphite and mica, with presence of vertical foliation. In the trench it is possible to notice the presence of quartz veins oblique to the foliation that contain manganese minerals and occur filling fractures. The host rock presents some recrystallization

in the contact with the veins. Samples LR44A and LR44B (Fig. 3B) are graphite schist with vertical foliation, while sample LR44C (Fig. 3C) was taken from an associated quartz vein (Fig. 3D), with manganese minerals, oriented N40E/75NW. The visual proportion between graphite and manganese mineral in this sample is 4:1. Each sample was between 10 and 20 cm long and weighed approximately 0.5 kg.

Fig. 3. Graphite schist sampling site. (A) Front view of trench; (B) Place where samples LR44A and LR44B were collected; (C) Sample LR44C, collected from quartz vein with presence of todorokite and manganite; (D) Quartz vein where sample LR44C was collected.

3.1 Petrography

Thin sections of the collected samples were prepared and examined under transmitted and reflected light microscopy at the Centro de Pesquisa (Research Centre) Professor Manoel Teixeira da Costa of Intitute of Geosciences of the Universidade Federal de Minas Gerais (CPMTC-IGC-UFMG), at Belo Horizonte, MG, Brazil.

The studied rocks are fine grained and have granolepidoblastic texture (Fig. 4). They are composed of quartz (50%), graphite (35%) and phengite (15%). Quartz is the dominant mineral in the composition and occurs in anhedral fractured grains. The second main component is graphite, presentedin aggregates (LR44A) and in layers parallel with foliation (LR44B). Phengite marks the foliation in both samples, but occurs in larger crystals in sample LR44B than in sample LR44A. The foliation is more evident in sample LR44B than it is in sample LR44A.

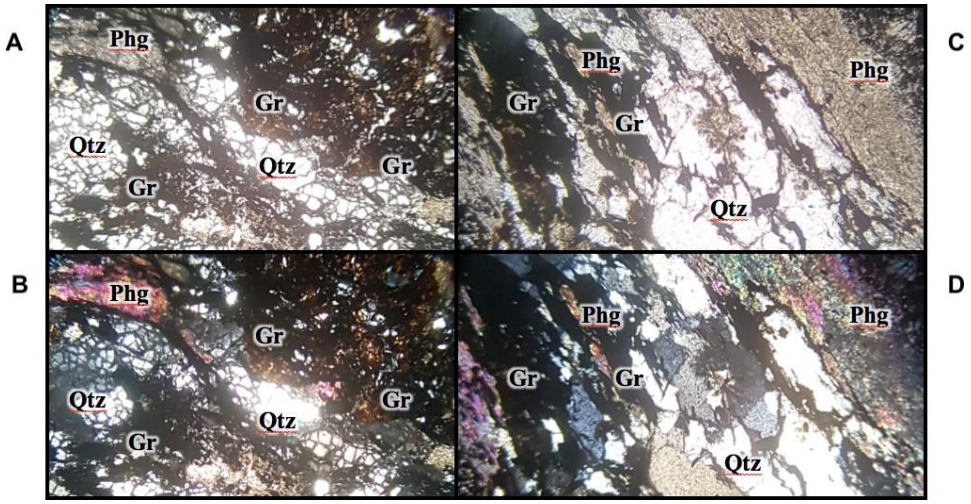

Fig. 4. Protomicrographies of samples LR44A (A, B) and LR44B (C, D) on plane polarized light (A, C) and crossed polarized light (B, D). Samples present granolepidoblastic texture. Graphite occurs in aggregates in sample LR44A, while in sample LR44B it occurs in layers parallel to foliation (marked by phengite). Mineral abbreviations, in accordance to Whitney and Evans (2010), are: Gr – graphite; Qtz – quartz; Phg – phengite.

3.2 X-ray diffraction (XRD)

The XRD analyses of graphite were performed in the X-ray Laboratory at CPMTC-IGC-UFMG. The mineral was previously isolated from other minerals of the graphite schist by brushing the graphite-rich portion of the rock, followed by graphite flotation in aqueous environment and drying of the floated grains. PANalytical XPert PRO diffraction instrument with theta-theta geometry was used to record the XRD data, using a Cu Kα X-ray source (40 kV and 45 mA). The step size and scan step settings were 0.02°, 2θ and 0.5 s. The high accuracy of the lattice parameter was guaranteed using Rietveld methods (Young 1993) to fit the diffraction data, with starting parameters close to realistic values and equally applied to both samples LR44A and LR44B. Fig. 5 shows the XRD results of sample LR44C, composed of todorokite and manganite instead of graphite. The XRD data from the graphite schist samples are organized in Table 1 and their respective diffractogram are presented in Fig. 6.

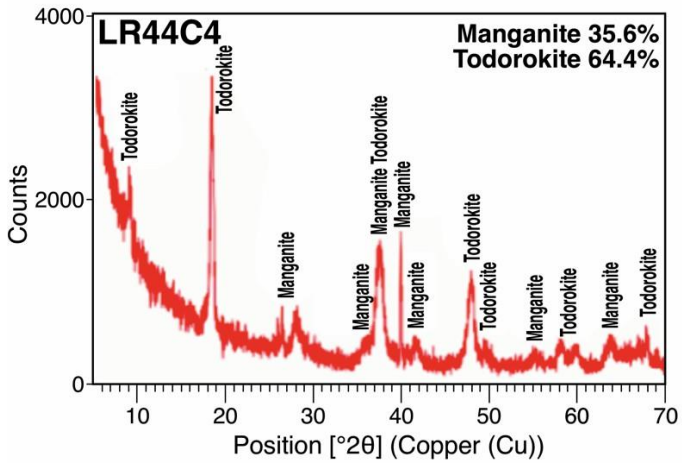

Fig. 5. Diffractogram of sample LR44C showing de presence of the biogenic Mn-rich minerals.

Table 1. X-ray diffraction data from LR44A and LR44B, graphite schist samples, where $d_{(002)}$ represents interplanar spacing, FWHM is the full width at half maximum of the G-band, $L_{c(002)}$ is the crystal size along stacking direction, GD is the graphitization degree and T is the peck metamorphic temperature.

X-ray diffraction data									
Sample	**2θ**	**d(002) (Å)**	**sd ±**	**FWHM (2θ)**	**Lc(002) (Å)**	**sd ±**	**GD**	**T(°C)**	**sd ±**
LR44A1	26.533	3.357	0.005	0.347	236	25	55	455	23
LR44A2	26.411	3.372	0.01	0.402	203	21	47	432	22
LR44A3	26.666	3.340	0.005	0.441	185	19	49	437	22
LR44A4	26.446	3.368	0.01	0.366	223	23	51	443	22
LR44B1	26.556	3.354	0.005	0.330	247	26	57	462	23
LR44B2	26.494	3.362	0.01	0.392	208	22	50	439	22
LR44B3	26.578	3.351	0.005	0.467	175	18	46	427	21
LR44B4	26.413	3.374	0.01	0.297	275	29	58	466	23

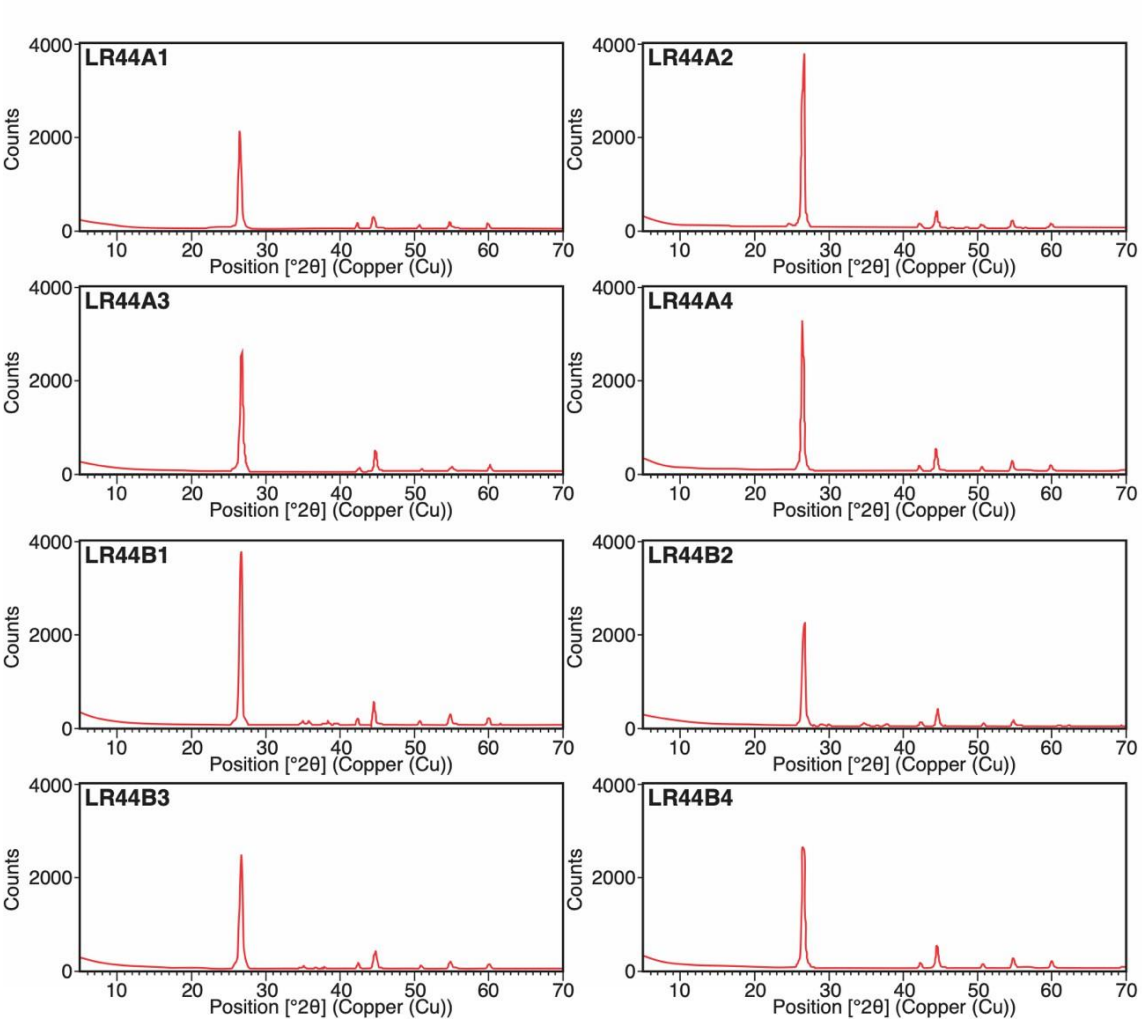

Fig. 6. Diffractograms of samples 44A and 44B showing graphite patterns. All peaks are from graphite.

To estimate the crystal size along stacking direction ($Lc_{(002)}$), we used the Equation 1 provided by Baiju et al. (2005).

$$L_{c(002)} = k\lambda/\beta_{(002)} \cos\theta \quad (1)$$

In this equation, k means the shape constant (0.9), λ is the X-ray wavelength in angstroms (1.5406), $\beta_{(002)}$ represents the full width at half maximum of the peak in radian and

θ correspond to the angle of diffraction in radians. The graphitization degree (GD) has been calculated using the equation from Tagiri (1981), were $d_{(002)}$ is the interplanar spacing:

$$GD = \{[d_{(002)} - 3.7] / [\log(L_{c(002)} / 1000)]\} \times 100 \quad (2)$$

Moreover, the equation from Wada et al. (1994) has been used to calculate the metamorphism temperature:

$$T(ºC) = 3.2 \times GD + 280 \quad (3)$$

The average temperature found for samples LR44A and LR44B were 442ºC and 449ºC respectively.

Graphs in Fig. 7 show correlations that could be done with the results obtained from the XRD data. Fig. 7A presents the a relationship between interplanar spacing ($d_{(002)}$) and crystallite size ($Lc_{(002)}$), that, in accordance with Tagiri and Oba (1986), can give information about the graphitization degree. Both samples LR44A and LR44B were classified as graphite as opposed to fully ordered graphite. The two samples presented similar XRD temperatures and are randomly arranged in the line that correlated graphitization degree with metamorphic temperature in the Fig. 7B.

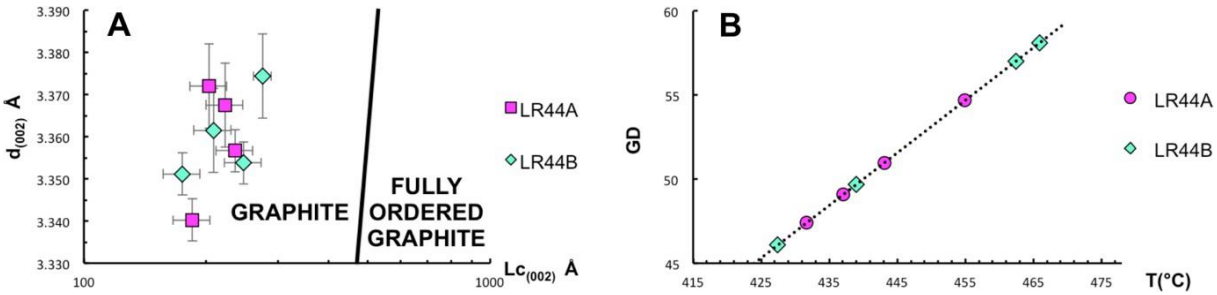

Fig. 7. (A) Interplanar spacing ($d_{(002)}$) versus crystallite size ($L_{c(002)}$) (Tagiri and Oba, 1986). All samples are classified as graphite, but they aren't full ordered; (B) Graphitization degree (GD) versus XRD data temperature (T) (Wada et al., 1994). Samples presented similar XRD temperature and are randomly arranged in the trendline.

3.3 Raman spectroscopy

The Raman spectroscopy analyses were performed in the Technological Center of Nanomaterials (CTnano) at Technological Park of Belo Horizonte — BHTec. The equipment used was a confocal microspore Alpha 300R WITec (Wissenschaftliche Instrumente und Technologie GmbH®, Ulm, Germany) equipped with Nd-YAG laser with double frequency (2.49 mW, λ = 532.2 nm). The same methodology as applied by Rantitsch et al. (2016) has been used, in which the spectra were obtained with 50× lens objective. Five scans in the 1,000–3,200 cm^{-1} spectra (first order = 1,000 – 2,000 cm^{-1}; second order = 2,200 – 3,200 cm^{-1}) were performed with an acquisition time of 30 s. The analyses were made using the powder extracted from both samples LR44A and LR44B.

In each sample, five fields were randomly selected (Fig. 8A, represented by squares),

in which three to five analyses were done per square field (Fig. 8B, represented by crosses). The results of Raman spectroscopy are presented in Table 2, and the respective spectrum are presented in Fig. 9 (sample 44A) and Fig. 10 (sample 44B).

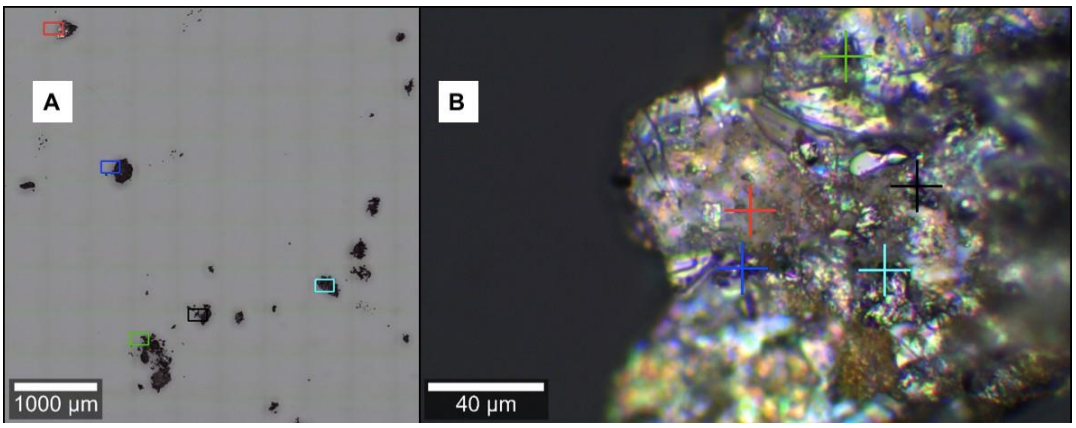

Fig. 8. Photomicrographs of graphite powder (extracted from sample LR44A) taken in PPL. (A) Selected fields for analyses represented with squares; (B) a random powder chosen for Raman analyses, in which each cross represents a spot of analyse.

Table 2. Raman spectroscopy data with values obtained by the IFORS method (Lünsdorf and Lünsdorf, 2016) from graphite schist samples LR44A and LR44B. G HWHM represents the width at half maximum of the G-band in cm^{-1}, R2 is the area ratio and T is the metamorphic peak temperature in ºC.

Raman spectroscopy data								
Sample	**G HWHM**	**sd ±**	**Center**	**sd ±**	**R2**	**sd ±**	**T ºC**	**sd ±**
LR44Aa1p1	7.94	0.42	1581.58	0.00	0.000	0.000	521	64
LR44Aa1p2	7.87	0.00	1581.58	0.00	0.067	0.000	496	63
LR44Aa1p3	7.78	0.00	1581.58	0.00	0.070	0.001	410	61
LR44Aa1p4	8.33	0.00	1581.58	0.00	0.120	0.000	492	63
LR44Aa1p5	8.91	0.00	1581.58	0.00	0.066	0.001	465	62
LR44Aa2p3	8.06	0.48	1581.58	0.00	0.000	0.000	488	63
LR44Aa3p1	7.90	0.00	1581.58	0.00	0.047	0.001	499	63
LR44Aa3p2	8.08	0.00	1584.06	0.00	0.140	0.161	497	63
LR44Aa3p3	7.67	0.00	1581.58	0.00	0.000	0.000	494	63
LR44Aa4p1	7.71	0.00	1581.58	0.00	0.000	0.000	476	63
LR44Aa4p3	7.78	0.00	1579.09	0.00	0.127	0.000	479	63
LR44Aa5p1	7.79	0.01	1581.58	0.00	0.119	0.000	501	63
LR44Aa5p2	7.85	0.00	1581.58	0.00	0.057	0.000	499	63
LR44Aa5p3	8.00	0.00	1574.12	0.00	0.118	0.001	487	63
LR44Ba1p1	8.89	0.00	1581.58	0.00	0.000	0.000	502	63
LR44Ba1p2	8.90	0.00	1583.28	0.00	0.216	0.000	492	63
LR44Ba1p3	8.78	0.00	1580.79	0.00	0.050	0.000	498	63
LR44Ba1p4	9.58	0.01	1582.45	1.44	0.044	0.001	491	63
LR44Ba2p1	8.12	0.00	1580.79	0.00	0.056	0.000	502	63
LR44Ba2p2	8.17	0.01	1575.81	0.00	0.060	0.000	493	63
LR44Ba2p3	8.46	0.00	1583.28	0.00	0.035	0.000	505	64
LR44Ba2p4	8.94	0.02	1578.30	0.00	0.081	0.000	481	63
LR44Ba3p3	8.01	0.00	1580.79	0.00	0.000	0.000	500	63
LR44Ba4p1	9.09	0.01	1583.28	0.00	0.144	0.002	496	63
LR44Ba4p2	9.82	0.00	1583.28	0.00	0.063	0.000	492	63
LR44Ba4p3	8.51	0.00	1588.78	0.00	0.088	0.000	499	63

LR44Ba5p1	8.36	0.00	1588.78	0.00	0.039	0.000	491	63
LR44Ba5p2	9.32	0.00	1588.78	0.00	0.052	0.000	491	63

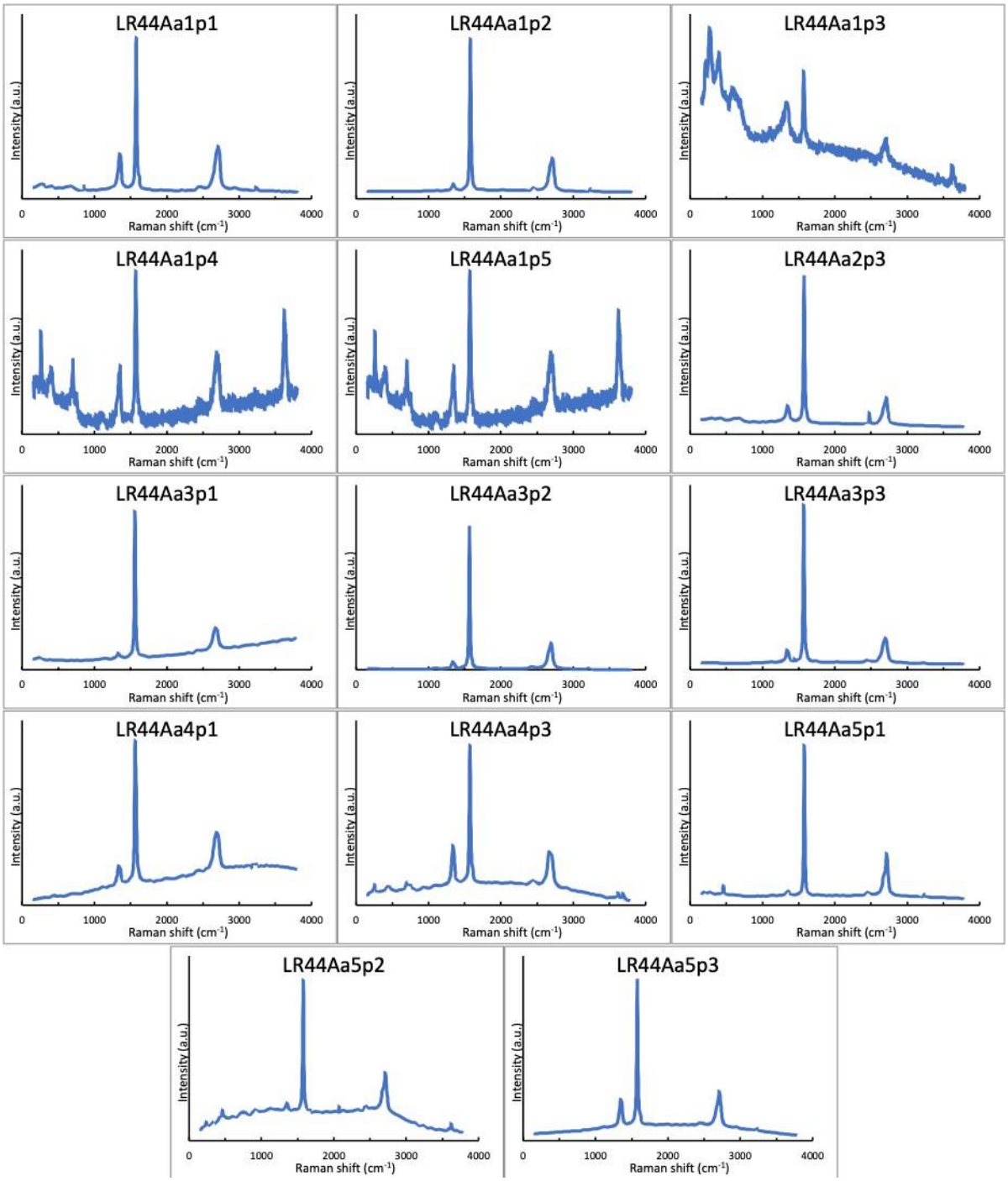

Fig. 9. Raman spectra of analyses made on sample 44A presenting graphite pattern. Some samples show some interference due the contamination of phengite.

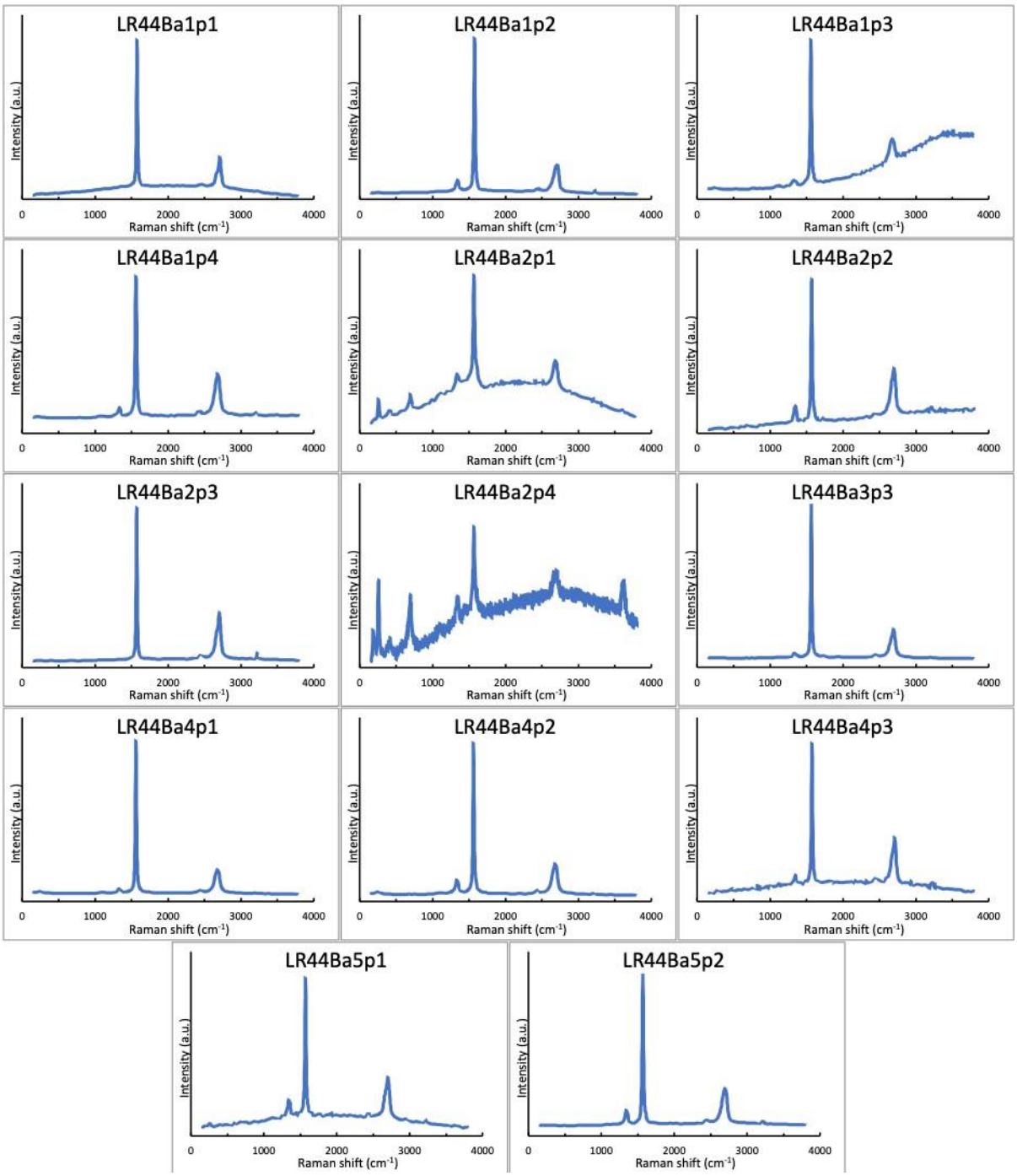

Fig. 10. Raman spectra of analyses made on sample 44B presenting graphite pattern. Some samples show some interference due the contamination of phengite.

The temperature has been calculated by using the Interactive Fitting of Raman Spectra (IFORS) method, provided by Lünsdorf and Lünsdorf (2016). The average temperatures found for each sample were 486°C for sample LR44A and 463°C for sample LR44B. The graphs from Fig. 11 classifies, according to Rantitsch et al. (2016), the metamorphic facies based on interplanar spacing and width at half maximum of the G-band (G HWHM) or area ratio (R2). The area ratio is calculated as described as Beyssac et al. (2002) using the first-order peaks at ~1,350 cm^{-1} (D1 band), ~1,580 cm^{-1} (G band), and ~1,610 cm^{-1} (D2 band), by the Equation 4:

$$R2 = D1/(G + D1 + D2) \quad (4)$$

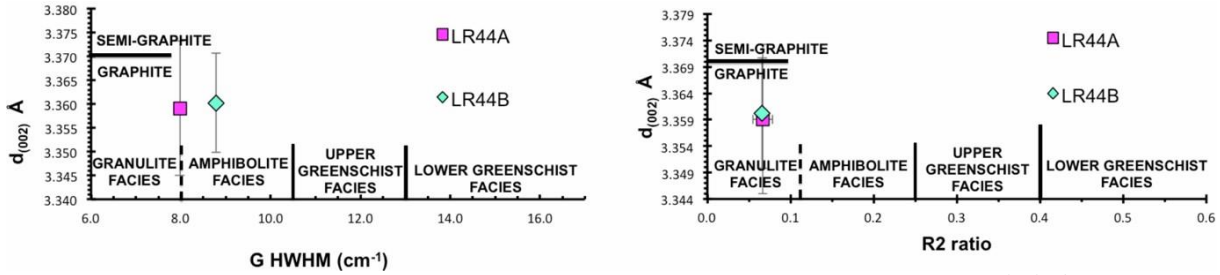

Fig. 11. (A) $d_{(002)}$ versus half width at half maximum of the G-band (G HWHM) (Beyssac et al. 2002, Kwiecińska and Petersen 2004, Rantitsch et al. 2016). Sample LR44A is classified as upper amphibolite facies and LR44B as amphibolite facies; (B) $d_{(002)}$ versus area ratio (R2) (Kwiecińska and Petersen 2004, Rantitsch et al. 2016). Both samples are classified as granulite facies.

The results, showed in Fig. 11, revealed that both samples present graphite. In Fig. 11A both samples are plotted in upper amphibolite facies, while in Fig. 11B they are classified as granulite. The reason why this divergence occurs is explored in the discussion section.

4. DISCUSSIONS

To characterize the graphite schist from Formiga, we correlate X-ray diffraction and Raman spectroscopy from samples LR44A and LR44B. The Table 3 compares metamorphic temperatures acquired from both methods that yielded temperatures around 460°C. According to Lünsdorf (2015), Raman analyses are reliable for temperatures between 330 and 600°C, so Raman data presented here are reliable. This temperature disagrees with the high metamorphic degree expected for the area (Chaves et al. 2015). However, it agrees with the results found by Miranda et al. (2019) for hydrothermal recrystallized graphite.

Table 3. Comparison between X-ray diffraction and Raman spectroscopy data from samples LR44A and LR44B of graphite schist. $d_{(002)}$ represents the interplanar spacing, GD is the graphitization degree, T is the metamorphic peak in ºC, G HWHM represents the width at half maximum of the G-band and R2 is the area ratio.

Sample	XRD							Raman						
	n	$d_{(002)}$	std	GD	std	T ºC	std	n	G HWHM	std	R2	std	T ºC	std
LR44A	4	3.359	0.014	50.5	3.1	442	10	14	7.976	0.066	0.067	0.012	486	63
LR44B	4	3.360	0.010	52.7	5.8	449	19	14	8.782	0.004	0.066	0.000	463	64

The XRD data (Tab. 1) was plotted in graphs to analyse the GD accordantly to its crystallinity. Fig. 7A correlates interplanar spacing ($d_{(002)}$A) and crystallite size ($L_{c(002)}$A), and, as suggested by Tagiri and Oba (1986), shows that both samples are classified as graphite between the fields of disordered graphite and fully ordered graphite. This corresponds to the temperatures which were found in this work, as graphite becomes fully ordered around 600°C (Beyssac et al. 2002, Lünsdorf 2015). The GD and XRD data temperature (T) are plotted using the equation for graphitization in pelitic rocks (Wada et al. 1994), and data from samples LR44A and LR44B behave similarly, leading to the conclusion that they both have been metamorphized under the same conditions.

The data acquired by Raman spectroscopy (Tab. 2) gave quite controversial results when plotted in graphs that classify the metamorphic facies as proposed by Rantitsch et al. (2016). Fig. 11A correlates the interplanar spacing $d_{(002)}$ and half width at half maximum of the G-band (G HWHM) and classifies the sample LR44B as related to the amphibolite facies while the sample LR44A to the upper amphibolite facies. Fig. 11B shows the correlation between $d_{(002)}$ and area ratio (R2 from Beyssac et al. 2002) in which both samples are classified as related to the granulite facies. This result was expected assuming the metamorphism considered for the area (Chaves et al. 2015), but it disagrees with the temperatures found by both methods. Also, the samples are classified as graphite (Kwiecińska and Petersen 2004) in both graphs presented in Fig. 11.

An explanation for why the temperatures found by the XRD and Raman methods (Tab. 1), for both graphite schist samples, disagrees with the syn-collisional metamorphism (Chaves et al. 2015), and the classifications based on crystallinity (Rantitsch et al. 2016), revealed in Fig. 11, could be associated with a post-collisional stage. In this phase, the reactivation of old faults creates open space for fluid percolation (Carvalho et al. 2017, Miranda et al. 2019). It is possible to observe quartz veins apparently related with this event (Fig. 3D). According to Miranda et al. (2019), hydrothermal process can decrease the crystallite size, placing the samples into high-grade metamorphic fields, even when they were metamorphized in much lower temperatures, that is, around 460°C. In their analyses, samples from hydrothermal recrystallized graphite had results similar to those presented here. They are classified as amphibolite facies in the correlation of Fig. 8A and granulite facies in the correlation of Fig. 11B, exactly as it happens to the samples analysed here.

The graphite schist from the Itapecerica region, which is adjacent to the present area of study, has biogenic origin (Miranda et al. 2019). As in Formiga area, todorokite (Mn-oxide mineral typical of deep-sea Mn nodules formed by microorganisms, as suggested by Lowenstam 1981) is also present. Given the geological and mineralogical similarities between the two areas, it is possible to assume that the graphite schist from Formiga also has biogenic origin. This carbonaceous material would have been deposited in an oceanic basin between the Campo Belo and Divinópolis complexes in the pre-collisional stage. During the Rhyacian-Orosirian orogeny, graphite schist would be metamorphized under granulite facies conditions and faults were formed. In post-collisional stage, the faults would have been reactivated turning into pathways to fluids which changed the graphite structure, decreased its crystallite size and changed the temperature signature to around 460°C.

5. CONCLUSION

The graphite schist from Formiga presented temperature around 460°C by the XRD and Raman analyses. The hydrothermalism associated with a post-collisional event explains the decrease in the crystallite size of the graphite mineral and its low temperature, while temperature typical of granulite facies was expected. The occurrence of todorokite in quartz veins and the presence of graphite with $\delta^{13}C$ between -21.23 and -27.89‰ in the adjacent area (Miranda et al. 2019) suggest a biogenic origin for the carbonaceous material that resulted in the graphite schist from Formiga.

6. ACKNOWLEDGEMENTS

We are grateful to the Institute of Geosciences of UFMG that avail the CPMTC laboratories. The second author thanks Fundação de Amparo à Pesquisa do Estado de Minas Gerais (FAPEMIG) for research financial support through the project APQ00654–16.

7. REFERENCES

Alkmim F.F. & Martins-Neto M.A. 2001. A Bacia Intracratônica do São Francisco: Arcabouço estrutural e cenários evolutivos. In: Martins-Neto M.A. & Pinto C.P. (eds). Bacia do São Francisco. Belo Horizonte, SBG-MG, p. 9-30.

Alkmim F.F. & Teixeira W. 2017. The Paleoproterozoic Mineiro Belt and the Quadrilátero Ferrífero. In: Heilbron, M., Alkmim, F., Cordani U.G. (eds.), The São Francisco Craton and its margins, Eastern Brazil. Regional Geology Reviews. Switzerland, Springer, p. 71-94.

Almeida F.F.M., Hasui Y., Brito Neves B.B., Fuck R.A. 1981. Brazilian structural provinces: An introduction. Earth-Science Reviews, 17(1-2): 1–29.

Ávila C.A., Teixeira W., Bongiolo E.M., Dussin I.A., Vieira T.A.T. 2014. Rhyacian evolution of subvolcanic and metasedimentary rocks of the southern segment of the Mineiro belt, São Francisco Craton, Brazil. Precambrian Research, 243:221–251.

Baiju K.R., Satish-Kumar M., Kagi H., Nambiar C.G., Ravinsankar M. 2005. Mineralogical characterization of graphite deposits from Thodupuzha-Kanjirappally belt, Madurai granulite block, Southern India. Gondwana Research, 8:223–230.

Baltazar O.F. & Zucchetti M. 2007. Lithofacies associations and structural evolution of the Archean Rio das Velhas greenstone belt, Quadrilátero Ferrífero, Brazil: A review of the setting of gold deposits. Ore Geology Reviews, 32:471-499.

Beyssac O., Goffé B., Chopin C., Rouzaud J.N. 2002. Raman spectra of carbonaceous material in metasediments: A new geothermometer. Journal of Metamorphic Geology, 20:859–871.

Burns R.G., Burns V.M., Stockman H.W. 1983. A review of the todorokite-buserite problem: implications to the mineralogy of marine manganese nodules. American Mineralogist, 68:972-980.

Buseck P.R. & Beyssac O. 2014. From organic matter to graphite: Graphitization. Elements, 10:421–426.

Campello M.S., Vaz B.B., Oliveira M.A.S., Ávila M.A.C. 2015. Folha Formiga (SF. 23-VB-III) Escala 1: 100.000. Projeto Fronteiras de Minas, CODEMIG/UFMG.

Carvalho B.B., Janasi V.A., Sawyer E.W. 2017. Evidence for Paleoproterozoic anatexis and crustal reworking of Archean crust in the São Francisco Craton, Brazil: A dating and isotopic study of the Kinawa migmatite. Precambrian Research, 291:98–118.

Chaves A.O., Campello M.S., Pedrosa-Soares A.C. 2015. Idade U-Th-PbT de monazitas do sillimanita-cordierita-granada-biotita gnaisse de Itapecerica (MG) e a atuação da orogenia Riaciano-Orosiriana no interior do Cráton São Francisco Meridional. Geociências, 34(3):324–334.

Dorr J.V.N. 1969. Physiographic, stratigraphic and structural development of the Quadrilatero Ferrifero, Minas Gerais, Brazil, U.S. Geological Survey Professional Paper, 641-A:110.

Farina F.A., Albert C., Lana C. 2015. The Neoarchean transition between medium and high-K granitoids: Clues from the Southern São Francisco Craton (Brazil). Precambrian Research, 266:375–394.

Gálvez M.E., Beyssac O., Martinez I., Benzerara K., Chaduteau C., Malvosin B., Malavieille J. 2013. Graphite formation by carbonate reductionduring subduction. Nature Geoscience, 6:473–477.

Harlow G.E. 1998. The nature of Diamonds. Cambridge, Cambridge University Press.

Kwiecińska B. & Petersen H. 2004. Graphite, semi-graphite, natural coke, and natural char classification-ICCP system. International Journal of Coal Geology, 57:99–116.

Lowenstam H.A. 1981. Minerals formed by organisms. Science, 211:1126-1131.

Lünsdorf, N.K. 2015. Geothermometry by Raman Spectroscopy of Dispersed Organic Matter. PhD thesis, University of Göttingen, Göttingen. 113 p.

Lünsdorf, N.K. & Lünsdorf, J.O. 2016. Evaluating Raman spectra of carbonaceous matter by automated, iterative curve-fitting. International Journal of Coal Geology, 160:51–62.

Luque F.J., Pasteris J.D., Wopenka B., Rodas M., Barrenechea J.F. 1998. Natural fluid-deposited graphite: Mineralogical characteristics and mechanisms of formation. American Journal of Science, 298:471–498.

Machado N., Schrank A., Noce C.M., Gauthier G. 1996. Ages of detrital zircon from Archean-Paleproterozoic sequences: Implications for greenstone belt setting and evolution of a Transamazonian foreland basin in Quadrilátero Ferrífero, southeast Brazil: Evidence from zircon ages by laser ablation ICP-MS. Earth Planetary Science Letters, 141:259–276.

Machado Filho L., Ribeiro M., Gonzales S.R., Schenini C.A., Santos Neto A., Palmeira R.C., Pires J.L., Teixeira W., Castro H.E.F. 1983. Geologia das folhas Rio de Janeiro (SF

23/24) escala 1:1.000.000, mapa e texto explicativo. RADAM Brasil, Ministério das Minas e Energia, Rio de Janeiro, 780 p.

Miranda D.A., Chaves A.O., Campello M.S., Ramos S.L.L.M. 2019. Origin and thermometry of graphites from Itapecerica supracrustal succession of the southern Sao Francisco Craton by C isotopes, X-ray diffraction, and Raman spectroscopy. International Geology Review, 61:1864-1875.

Moreira H., Lana C., Nalini H.A. 2016. The detrital zircon record of an Archaean convergent basin in the Southern São Francisco Craton, Brazil. Precambrian Research, 275:84–99.

Noce C.M., Machado N. Teixeira W. 1998. U-Pb Geochronology of gneisses and granitoids in the Quadrilatero Ferrıfero (Southern São Francisco Craton): Age constraints for Archean and Paleoproterozoic magmatism and metamorphism. Revista Brasileira de Geociencias, 28:95–102.

Noce C.M., Pedrosa-Soares A.C., Silva L.C.D., Alkmim F.F. 2007. O embasamento arqueano e paleoproterozóico do orógeno Araçuaí. Geonomos, 15:17-23.

Rantitsch G., Lämmerer W., Fisslthaler E., Mitsche S., Kaltenböck H. 2016. On the discrimination of semi-graphite and graphite by Raman spectroscopy. International Journal of Coal Geology, 159:48–56.

Simandl G.J., Paradis S., Akam C. 2015. Graphite deposit types, their origin, and economic significance. In: Simandl G.J. & Neetz M. (Eds.), Symposium on Strategic and Critical Materials Proceedings, Victoria, British Columbia Geological Survey, p. 163-171.

Tagiri M. 1981. A measurement of the graphitizing degree by the X-ray powder diffractometer. Journal of Mineralogy, Petrology and Economic Geology, 76:345–352.

Tagiri M. & Oba T. 1986. Hydrothermal syntheses of graphite from bituminous coal at 0.5–5 kbar water vapor pressure and 300–600°C. Journal of Mineralogy, Petrology and Economic Geology, 81:260–271.

Teixeira W., Carneiro M.A., Noce C.M., Machado N., Sato K., Taylor P.N. 1996. Pb, Sr and Nd isotope constraints on the Archean evolution of gneissic-granitoid complexes in the southern São Francisco Craton, Brazil. Precambrian Research, 78:151-164.

Teixeira W., Ávila C.A., Dussin I.A., Corrêa Neto A.V., Bongiolo E.M., Santos J.O.S., Barbosa N. 2015. Zircon U-Pb-Hf, Nd-Sr constraints and geochemistry of the Resende Costa Orthogneiss and coeval rocks: New clues for a juvenile accretion episode (2.36–2.33 Ga) in the Mineiro belt and its role to the long-lived Minas accretionary orogeny. Precambrian Research, 256:148–169.

Teixeira W., Oliveira E.P., Peng P., Dantas E.L., Hollanda M.H.B.M. 2017. U-Pb geochronology of the 2.0 Ga Itapecerica graphite-rich supracrustal succession in the São Francisco Craton: Tectonic matches with the North China Craton and paleogeographic inferences. Precambrian Research, 293:91–111.

Wada I.H., Tomita T., Iuchi K., Ito M., Morikiyo T. 1994. Graphitization of carbonaceous matter during metamorphism with reference to carbonate and pelitic rocks of contact

and regional metamorphism, Japan. Contributions to Mineralogy and Petrology, 118:217–228.

Whitney D.L. & Evans B.W. Abbreviations for names of rock-forming minerals. American Mineralogist, 95:185-187.

Wintsch R.P., O'Connel A.F., Lansom B.L., Wiechmann, M.J. 1981. Evidence for the influence off CH4 on the crystallinity of disseminated carbon in greenschist facies rocks, Rhode Island, USA. Contributions to Mineralogy and Petrology, 77:207–213.

Young R.A., 1993. The rietveld method. International Union of Crystallography. New York, Oxford University Press, 298 p.

ARTICLE II – Petrology, geochemistry and monazite U-Th-Pb ages of West Água Rasa metagranites from Southern São Francisco Craton – Brazil

Authors: Luiza Carneiro de Rezende[a], Alexandre de Oliveira Chaves[a].

[a] Geology Department, Institute of Geosciences, Federal University of Minas Gerais (UFMG), Belo Horizonte, Brazil

Published in periodic Geociências (São Paulo. Online).

DOI: https://doi.org/10.5016/geociencias.v40i04.16013

ABSTRACT

During the transition of Rhyacian to Orosirian periods a collision between the Archean Divinópolis and Campo Belo metamorphic complexes occurred followed by the collapse of the orogen. The Statherian period is marked by a huge intraplate magmatic event that is represented in the area by the Para de Minas dyke swarm. Peraluminous granitoid occurrences are reported in the region of Formiga and Itapecerica (Minas Gerais – Brazil), surrounding high metamorphic grade khondalitic paragneisses. To contribute to the understanding of the tectonic context of the Southern São Francisco Craton during the Paleoproterozoic era, these granitic rocks are studied based on petrographic, geochemical, and monazite U-Th-Pb geochronological analyzes. They were characterized as S-type (metasedimentary origin) peraluminous metamonzogranites, with crustal geochemical signature, and genesis related to anatexis in syn- to post-colisional environment. The geochronological results yelded two groups of Orosirian (~1,90 Ga) and Statherian (~1,78 Ga) ages. These results are related, respectively, to the collapse of the Rhyacian-Orosirian orogen and to the regional warming, associated with the Avanavero-Xiong'er LIP that is represented in the area by the Pará de Minas dykes swarm.

KEYWORDS: Anatexis, Monazite U-Th-Pb geochronology, Paleoproterozoic, São Francisco Craton.

1. INTRODUCTION

Granite is an igneous coarse-grained rock, composed mostly by quartz, alkali-feldspar, plagioclase, and mica (Read, 1943). Granitic rocks are the most abundant igneous rocks on the Earth's continental crust and are found in various tectonic settings. They can be formed in orogenic and continental collision zones, anorogenic intraplate settings, mid-ocean ridges, ophiolite complexes, and also as plutons (Gill, 2010). An interesting origin granitic magma can present is by anatexis.

Anatexis is the process in which magma is formed by partial melting of crustal rocks (Ashworth, 1985). It plays an important role of active deformation and emplacement of crustal

granites (Brown and Solar, 1998), especially when it comes from sediments (Harris et al., 2000). Different geochemical signature can evidence the supracrustal origin from granites (Frost et al., 2001; Whalen et al., 1987; Chappell and White, 2001; Laurent et al., 2014) and can relate to different tectonic setting (Batchelor and Bowden, 1985; Pearce, 1996).

Accordantly to Miranda et al. (2020) there are occurrences of metagranites with sedimentary origin, named Água Rasa, in the southern portion of the São Francisco Craton (SFC) (Fig. 1B) in the region of Itapecerica (Minas Gerais – Brazil) (Fig. 1B). They analyzed those rocks and, with geochemical and geochronological data, associated their origin to the anatexis of supracrustal sequences, process related to the Rhyacian-Orosirian event reported in this area (Chaves et al., 2015; Carvalho et al., 2017; Miranda et al., 2020; Chaves, 2021).

Based on gamma spectrometric image (Fig. 1C), metagranite samples that occurs between Formiga and Itapecerica (Fig. 1A) were studied in this paper. The study aims to characterize the nature, origin, and age of what was called West Água Rasa Granite, using petrography, geochemistry, and monazite U-Th-Pb geochronology. The results are used to corroborate to the understanding of the Paleoproterozoic tectonic context in the southern SFC.

2. GEOLOGICAL SETTING

The southern part of the SFC (A) is composed by an Archean crust (3.5 – 2.6 Ga) that is constituted mostly by granite-gneisses rocks (Farina et al., 2015; Teixeira et al., 2017) and rocks from Rio das Velhas Supergroup, that are greenstone belts formed by mafic-ultramafic rocks, intermediate-felsic volcanic and volcanoclastic rocks (Noce et al., 1998) and terrigenous sediments (Dorr, 1969; Baltazar and Zucchetti, 2007).

Above the basement, that comprehends Campo Belo, Divinópolis, Bonfim and Belo Horizonte metamorphic complexes (Machado Filho et al., 1983; Teixeira et al., 1996), occurs the supracrustal sequence that includes the Minas Supergroup and Bambuí Group. The first unit is formed by Paleoproterozoic clastic-chemical metasedimentary rocks, with minimum deposition around 2.0 Ga, and also the typical banded iron formations from the Quadrilátero Ferrífero (Machado et al., 1996; Moreira et al., 2016). Above occurs the Neoproterozoic pelitic-carbonate sedimentary rocks from Bambuí Group (Alkmim and Martins-Neto, 2001). All the southern SFC is crosscuted by mafic dykes (Chaves, 2013).

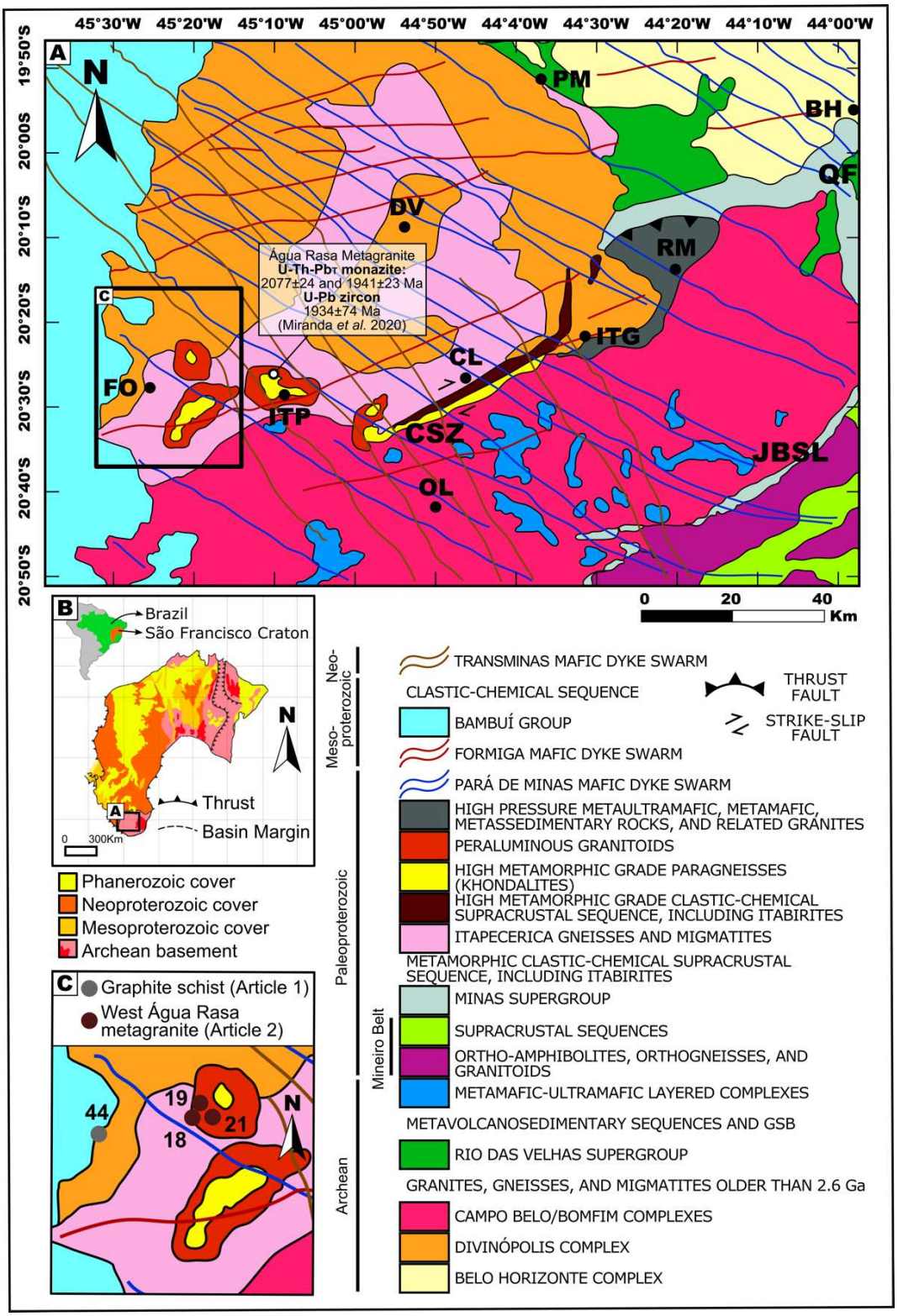

Fig. 1. (A) Geological map of the Southern São Francisco Craton interpreted from geophysics,, with the area of study highlighted. CSZ – Cláudio Shear Zone, JBSL – Jeceaba-Bom Sucesso Lineament, QF – Quadrilátero Ferrífero, Cities: BH – Belo Horizonte, CL – Cláudio, DV – Divinópolis, FO – Formiga, ITG – Itaguara, ITP – Itapecerica, OL – Oliveira, PM – Pará de Minas, RM – Rio Manso. Modified after Chaves and porcher (2020). (B) São Francisco Craton simplified map, with its Southern region highlighted. Modified after Drummond et al. (2015). (C) K-Th-U ternary gamma spectrometric image of the area of study with the samples collecting sites highlighted (CPRM-CODEMIG, 2014).

An orogeny that occurred between the Rhyacian and Orosirian resulted in extensive reworking of the margins of the southern portion of the SFC (Noce et al., 2007) and is also

responsible for the formation of the Mineiro Belt (Noce et al., 1998; Ávila et al., 2014; Teixeira et al., 2015). The existence of a Paleoproterozoic event in the Itapecerica region was firstly suggested by Chaves et al. (2015) based on chemical ages found in monazites from sillimanite-cordierite-garnet-biotite gneiss (graphite-rich khondalitic rocks) and then confirmed by Carvalho et al. (2017) with isotopic ages of 2.05-2.03 Ga (U-Pb) found in zircons from the interior of the basement. Miranda et al. (2020) studied Água Rasa metagranites (Fig. 1A), rocks that occur around the occurrences of khondalite, in which isotopic ages of zircons yield upper intercept of 1934 ± 74 Ma and chemical ages of monazites yield mean ages of 1941 ± 23 Ma and 2077 ± 24 Ma.

The area of the study (Fig. 1A) is located in Formiga region, close to Itapecerica. This area was described by Carneiro and Barbosa (2008) as containing Mesoproterozoic gneisses, metagranitoids, amphibolites, mafic, metaultramafic and metacharnocktic rocks, recrystallized under the conditions of amphibolite to granulite facies (Fernandes and Carneiro, 2000). Elliptical anomalies, visible on gamma-ray ternary K-Th-U map (Fig. 1C), are resulted of the presence of khondalitic graphite-rich rocks and banded iron formations and are contoured by metagranites known as Água Rasa, which are the object of study of this research.

3. METHODS

The samples were collected from three different sites (Fig. 1C) located northeast from Formiga (20º24’45.4”S, 45º22’30.9”W). Six samples (18A, 18B, 19A, 19B, 21A and 21B) of West Água Rasa metagranite were used for petrographic and geochemical investigations and sample 21A was also used for geochronological analyses.

3.1 Petrography

Six thin sections were prepared and examined under transmitted and reflected light microscopy at the CPMTC-UFMG (Professor Manoel Teixeira da Costa Research Centre of the Federal University of Minas Gerais).

3.2 Whole Rock Geochemistry

Six granite samples have been sent to whole rock geochemistry analyses in SGS-Geosol Laboratory. They were milled in tungsten mill, melted with lithium metaborate and diluted by nitric digestion. ICP-OES (Optical Emission Spectrometry with Inductively Coupled Plasma was used to analyze major elements and five trace elements (Ba, Sr, Zn, Zr and V), with detection limits of 0.01% and between 5 and 10 ppm, respectively. Other trace elements and rare earth elements were analyzed by ICP-MS (Inductively Coupled Plasma Mass Spectrometry) with detection limits ranging from 0.02 to 5 ppm. The loss on ignition (LOI)

was made by mass difference after heating at 1000ºC. The geochemical data was examined using Microsoft Excel supplement Geoplot (Zhou and Li, 2006).

3.3 Monazite mineral chemistry and U-Th-Pb$_T$ geochronology

Three different monazite grains from a granite sample were analyzed in polished thin section using a JXA-8900 JEOL electron microprobe (EMP), at Microanalysis Laboratory of the Microscopy Centre at Federal University of Minas Gerais (LMA-CM-UFMG). Standards and quantitative wavelength dispersive X-ray spectroscopy (WDS) analytical parameters were used as described by Chaves et al. (2013). To correct the effects of the matrix on the composition and pattern differences, a model proposed by Toya et al. (1984) was applied using ZAF factors. The corrections of X-ray peaks overlapping between Y and Pb were not corrected due to the absence of measurement in PbMa (Lead M alpha), occurring only in PbMb (Lead M beta). The interference of ThMz (Thoruim M gamma) on the measured UMb (Uranium M beta) was correct in order to avoid errors in the obtained ages. The correction was made as suggested by Chaves et al. (2013), following Scherrer et al. (2000) but adapted to the conditions of the LMA-UFMG, as follows:

$$U_{CORRECTED} = U_{MEASURED} - (0.006365 \times Th_{MEASURED}) \quad (1)$$

The software EPMA Dating (Pommier et al., 2004) was used to calculate the chemical U-Th-P$_T$ ages and associated errors. The average ages were calculated using Isoplot/Ex add-in (Ludwig, 2003). The equation used to age calculation was:

$$Pb = \{Th \times [\exp(\lambda_{232}T) - 1] \times (M_{208}/M_{232})\} + \{U_C \times [\exp(\lambda_{238}T) - 1] \times (M_{206}/M_{238}) \times 0.9928\} + \{U_C \times [\exp(\lambda_{235}T) - 1] \times (M_{207}/M_{235}) \times 0.0072\} \quad (2)$$

Where U_C (U corrected), Th and Pb are concentrations in ppm; T is age in Ma; M_{206}, M_{207}, M_{208}, M_{208}, M_{238}, M_{232} are, respectively, the atomic of ^{206}Pb, ^{207}Pb, ^{208}Pb, ^{235}U, ^{238}U, ^{232}Th; $\lambda_{232} = 0.49475 \times 10 - 4$ Ma^{-1}; $\lambda_{238} = 1.55125 \times 10 - 4$ Ma^{-1}; $\lambda_{235} = 9.8485 \times 10 - 4$ Ma^{-1} (Pommier et al., 2004).

4. RESULTS

4.1 Petrography

The samples (Fig. 2A and D) of West Água Rasa metagranite present similar mineralogical assemblage, distinguishing only in the mineral percentage and texture. They have phaneritic texture and have as main minerals quartz, plagioclase, microcline and micas, more biotite than muscovite (around 10%) and present apatite, zircon and opaques as accessory minerals. Monazite appears only in sample 21A. Samples from sites 18 and 21 (Group A) (Fig. 2B and C) are fine to medium grained with more microcline while samples collected from site

19 (Group B) (Fig. 2E and F) are coarser grained and present more plagioclase. In the Group A samples, quartz occurs as small to medium grains in which the medium grains are anhedral, fractured, with undulose extinction and the smaller are rounded, some occurring as myrmekite with plagioclase. Microcline occurs in subhedral medium grains with tartan twinning, which some presenting perthitic textures. Plagioclase also occurs in medium grains; however, they present strong saussurite alteration. Biotite grains are small, euhedral and slightly oriented, while muscovite is rare and occurs in even smaller elongated grains. In Group B samples all minerals occur coarser, even biotite. Quartz presents large recrystallized grains with undulose extinction. Plagioclase and microcline are presented in subhedral to euhedral grains, in which few microcline grains may present perthitic texture. Biotite occurs in medium subhedral to euhedral grains and are often altered to chlorite. Muscovite presents lamellar habit. The modal estimates are in Table 1 and the representation of the six samples are plotted in the Streckeisen diagram (Fig. 3A) (Streckeisen, 1974), where West Água Rasa metagranite is classified as monzogranite.

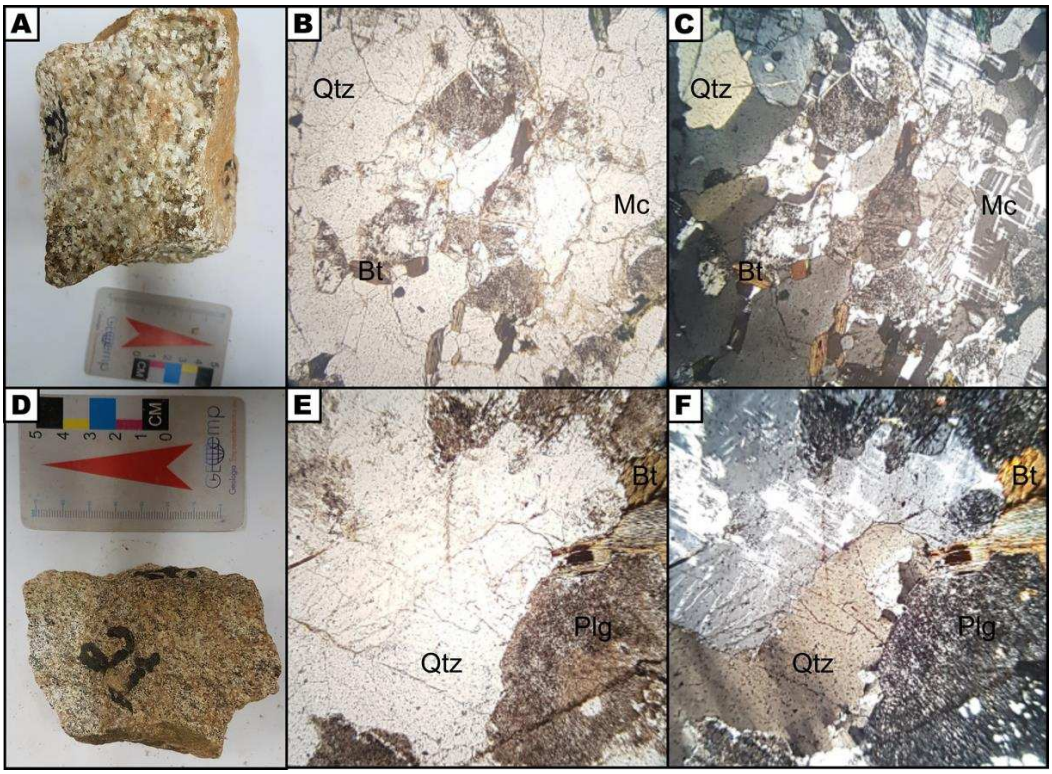

Fig. 2. Hand samples (A, D) and protomicrographies of samples 21 (A, B, C) and 19 (D, E, F) on plane polarized light (B, E) and crossed polarized light (C, F). Mineral abbreviations, in accordance to Whitney and Evans (2010), are: Bt: biotite; Mc: microcline; Plg: plagioclase; Qtz: Quartz.

Table 1. Percentage of mineral modal composition of West Água Rasa metagranite samples.

	Mineral modal composition (%)		
Sample	**Quartz**	**Plagioclase**	**Alkali feldspar**
18A	41	25	34
18B	34	28	38
19A	44	33	23
19B	42	38	20
21A	39	28	33
21B	37	26	37

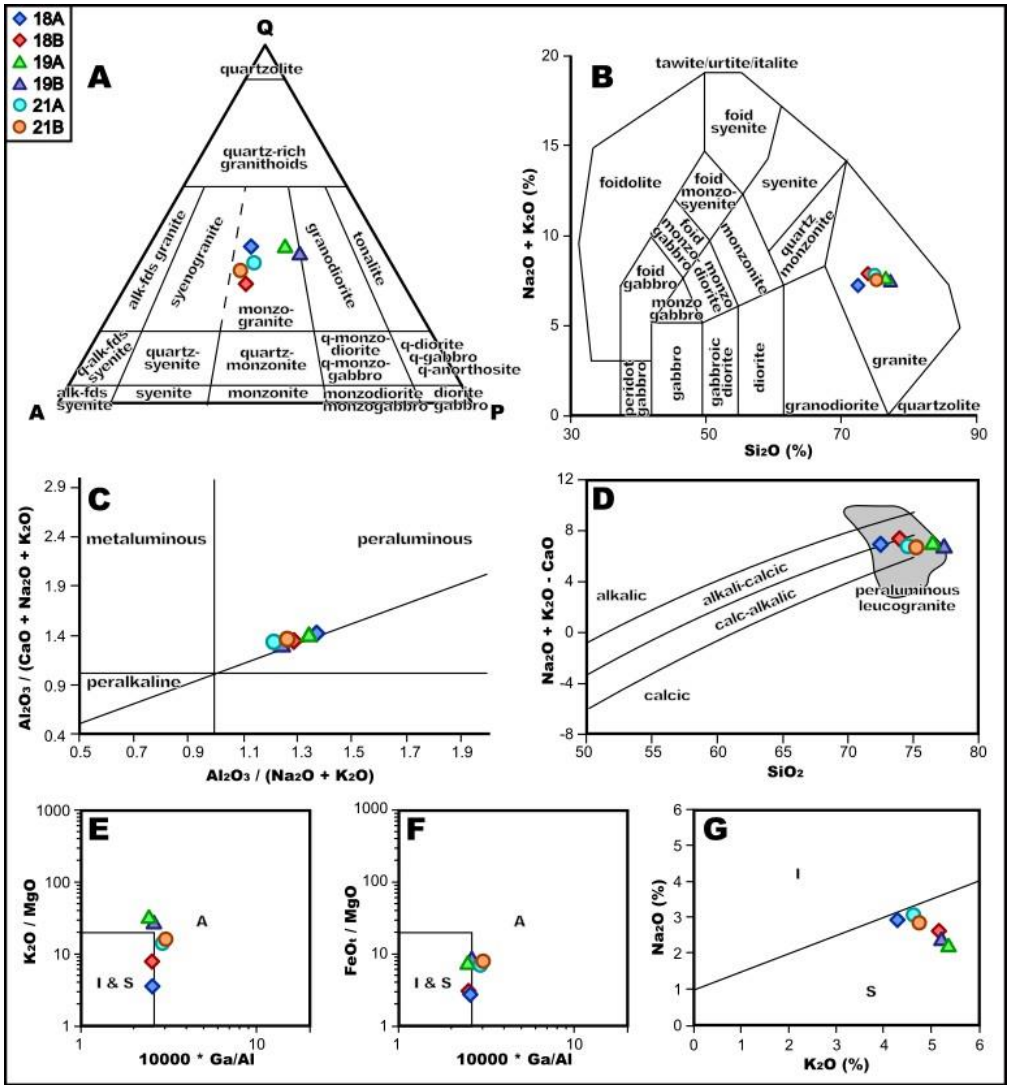

Fig. 3. Lithochemical data from West Água Rasa metagranite plotted on classification diagrams. (A) QAP modal diagram from Streckeisen (1974). (B) Total Alkalis versus Silica (TAS – Middlemost, 1994). (C) Diagram A/CNK- A/NK (Maniar and Piccoli, 1989). (D) Na2O + K2O + CaO vs. SiO2 (wt%) from Frost et al. (2001). (E and F) Anorogenic granite classification diagrams (Whalen et al., 1987). (G) Division between I and S-type of granites (Chappell and White, 2001).

4.2 Whole-rock geochemistry

All whole-rock geochemistry data are organized in Table 2. West Água Rasa metagranite is classified as granite in TAS diagram (Middlemost, 1994) (Fig. 3B) It is a peraluminous (Maniar and Piccoli, 1989) (Fig. 3C) leucogranite also plotted in the field of calc-alkalic rocks (Frost, 2001) (Fig. 3D). In Whalen et al. (1987) diagrams for anorogenic granites, the samples were plotted of the edge of the fields of A-type and I and S-types (Fig. 3E and F), while based in Chappell and White (2001) they were classified as S-type (Fig. 3G). The chondrite-normalized REE patterns (Sun and McDonough, 1989) presented enrichment in light rare earth elements (LREE) and Eu anomaly, positive in samples 19A and 19B, and negative in samples 21A and 21B and slightly negative in samples 18A and 18B (Fig. 4A). In the multi-elemental variation diagram normalized to chondrite (Sun and McDonough, 1989) the same Eu behavior is observed. Furthermore, samples 18A, 18B, 21A and 21B showed negative anomalies of Sr, while the opposite is observed in samples 20A and 20B (Fig. 4B). All samples plotted between syn-collisional to post-orogenic fields in Batchelor and Bowden (1985) diagram (Fig. 4C). In Pearce (1996) tectonic diagram (Fig. 4D), samples 18A, 18B, 19A and 19B plotted in the edge between syn-collisional to volcanic arc granites, while samples 21A and B plotted in the post-collision granites field. Finally, accordantly to the ternary diagram (Fig. 4E) from Laurent et al. (2014), all samples are granites derived from metasediments.

Table 3. Whole rock composition of West Água Rasa metagranite samples.

Sample	**Major Elements**											
	SiO2	**TiO2**	**Al2O3**	**Fe2O3**	**MnO**	**MgO**	**CaO**	**Na2O**	**K2O**	**P2O5**	**LOI**	**Total**
Detection Limit (%)	0.01	0.01	0.01	0.01	0.01	0.01	0.01	0.01	0.01	0.01	-45	
18A	72.48	0.29	13.28	2.92	0.03	1.18	0.31	2.96	4.27	0.09	1.71	99.52
18B	73.96	0.19	13.07	1.92	0.02	0.66	0.3	2.64	5.14	0.06	1.08	99.04
19A	76.83	0.06	13.43	1.25	0.02	0.16	0.54	2.25	5.34	0.01	1.08	100.97
19B	77.35	0.09	12.59	1.58	0.02	0.19	0.63	2.36	5.19	0.06	0.89	100.95
21A	74.68	0.23	13.31	2.23	0.03	0.32	0.92	3.09	4.6	0.08	0.66	100.15
21B	75.24	0.21	13.24	2.26	0.03	0.3	0.79	2.83	4.72	0.04	1.17	100.83
Sample	**Trace Elements**											
	Rb	**Ba**	**Sr**	**Zr**	**Nb**	**Y**	**Ni**	**Co**	**Hf**	**Ta**	**Th**	**U**
Detection Limit (PPM)	**0.02**	**10**	**10**	**10**	**0.05**	**0.05**	**5**	**0.5**	**0.05**	**0.05**	**0.01**	**0.05**
18A	113.5	838	113	277	8.74	6.88	2	7.3	6.45	0.38	25.9	2.89
18B	138.4	980	125	170	7.2	4.77	2	4.9	4.75	0.48	21.1	2.49
19A	171.8	1068	155	19	4.31	6.12	2	1.6	0.35	0.58	9.5	3.42
19B	153.6	914	149	46	4.36	7.15	2	1.8	1.4	0.56	8	4.77

21A	216.9	592	119	181	13.29	22.13	2	2.7	5.24	0.83	33.6	10.89	
21B	223.2	642	113	186	14.89	23.54	2	2.7	5.1	0.99	30.7	8.94	

Sample	**Rare Earth Elements**												
	La	**Ce**	**Pr**	**Nd**	**Sm**	**Eu**	**Gd**	**Tb**	**Dy**	**Ho**	**Er**	**Tm**	**Yb**	**Lu**
Detection Limit (PPM)	**0.1**	**0.1**	**0.05**	**0.1**	**0.1**	**0.05**	**0.05**	**0.05**	**0.05**	**0.05**	**0.05**	**0.05**	**0.1**	**0.05**
18A	75.9	113.9	14.08	48.5	7.7	1.17	4.87	0.48	2.36	0.29	0.88	0.1	0.6	0.08
18B	52.1	74.8	9.45	32.8	5.4	1.06	3.59	0.36	1.7	0.24	0.61	0.07	0.5	0.06
19A	7.2	12.9	1.2	5.2	1.3	0.66	1.15	0.19	1.31	0.27	0.87	0.11	0.9	0.11
19B	5.7	8.9	0.97	4.3	1.1	0.67	1.15	0.18	1.38	0.27	0.98	0.14	1	0.14
21A	47.2	95.3	10.51	40.4	8.3	0.68	6.41	0.9	5.18	0.9	2.64	0.32	2.2	0.29
21B	44	92.5	9.9	38.2	7.8	0.7	6.15	0.87	5.66	0.9	2.84	0.32	2.6	0.32

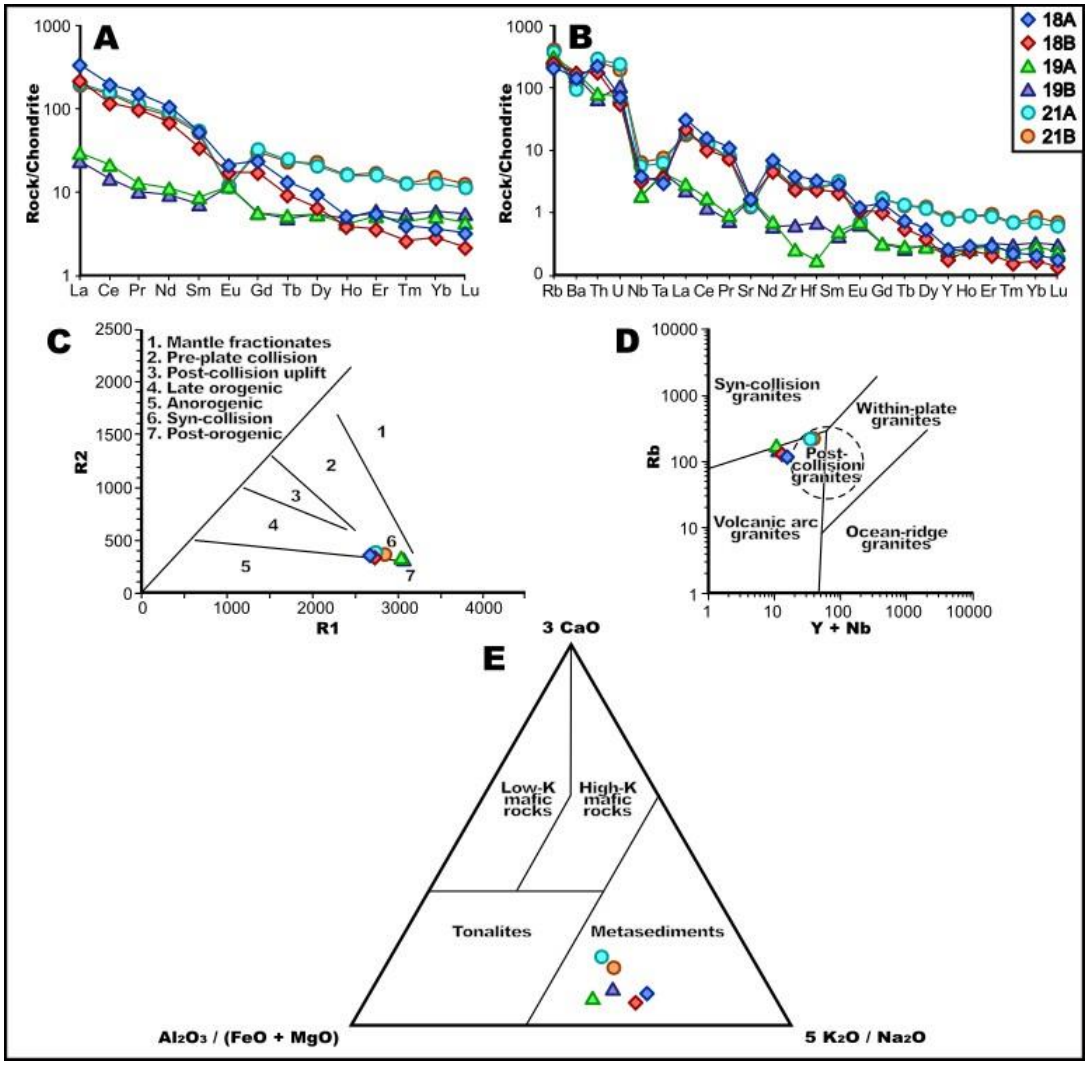

Fig. 4. (A) Chondrite-normalized REE patterns from Sun and McDonough (1989). (B) Multi-elemental spider diagram normalized to N-MORB from Sun and McDonough (1989). (C) R1-R2 diagram (Batchelor and Bowden, 1985). (D) Rb vs. Y+ Nb tectonic diagram from Pearce (1996). (E)Ternary diagram proposed by Laurent *et al.* 2014).

4.3 Monazite U-Th-Pb$_T$ geochronology

Monazite grains from sample 21A (West Água Rasa metagranite) are subhedral and very fractured and they show corroded aspect. Backscattered-Electron imaging don't show significative zoning (Fig. 5). According to the chemical data (Table 3), the grains are classified as monazite-(Ce). Three grains (21-mon-01, 21-mon-02 and 21-mon-03) were analyzed with 9 to 10 spots each. Each grain presented half the spots with Statherian age and the others yield Orosirian age (Table 4). The grain 21-mon-01 revealed mean ages of 1778 ± 22 Ma (95% conf., MSWD = 0.53; probability = 0.71) and 1946 ± 27 Ma (95% conf., MSWD = 1.00; probability = 0.39). The mean ages found in grain 21-mon-02 were 1789 ± 20 Ma (95% conf., MSWD = 0.69; probability = 0.60) and 1871 ± 36 Ma (95% conf., MSWD = 1.2; probability = 0.29). The last grain, 21-mon-03, yield mean ages of 1784 ± 19 Ma (95% conf., MSWD = 0.097; probability = 0.98) and 1904 ± 19 (95% conf., MSWD = 0.12; probability = 0.97) (Fig. 5). The mean Statherian and Orosirian ages found for all grains are, respectively, 1784±20 and 1907±27 Ma.

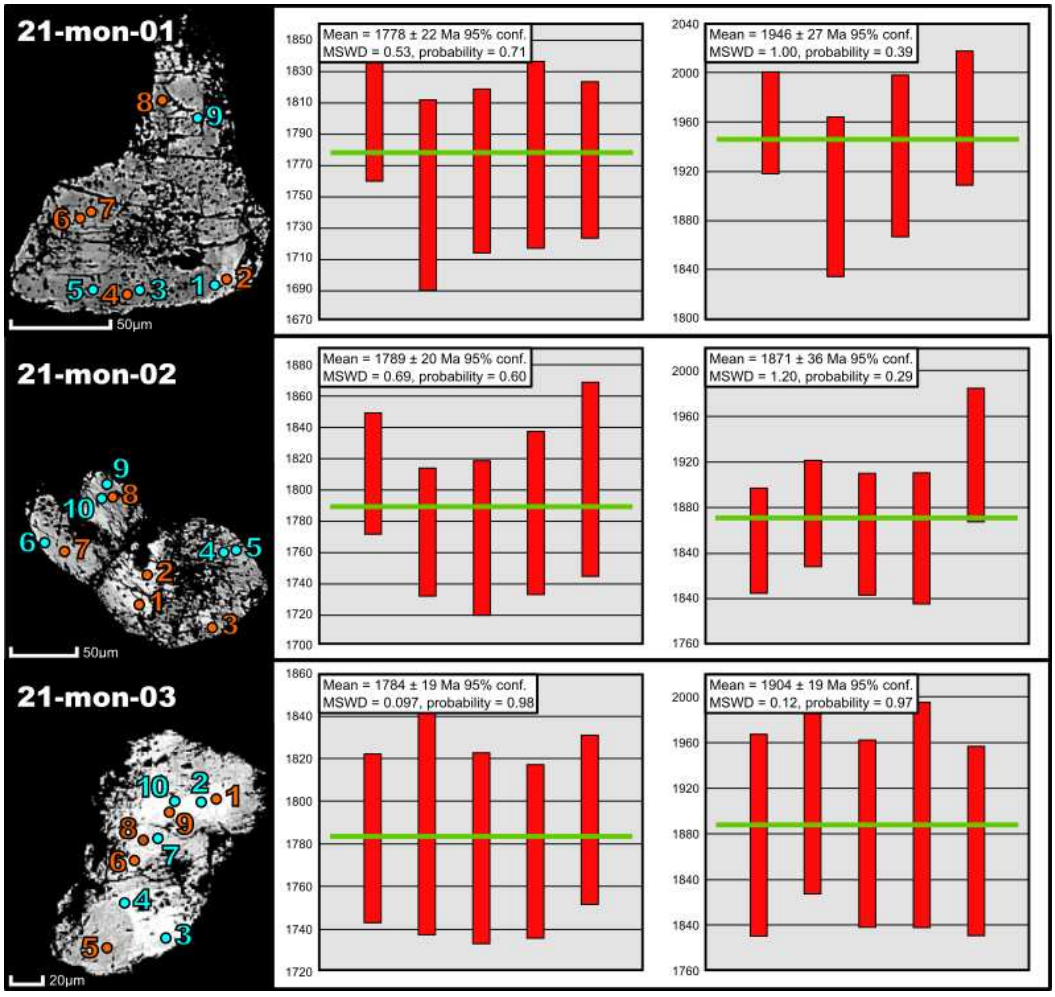

Fig. 5. Backscattered-Electron imaging of monazite grains from sample 21 with respective mean Statherian and Orosirian ages.

Table 3. Monazite from sample 21 (West Água Rasa metagranite) chemical data.

West Água Rasa monazite from sample 21

	P2O5	SiO2	ThO2	UO2	Y2O3	La2O3	Ce2O3	Pr2O3	Nd2O3	Sm2O3	Gd2O3	Dy2O3	CaO	PbO	Total
21-mon-01															
1	24.7	3.264	13.5	0.574	2.865	10.86	25.64	2.511	9.497	2.318	1.526	0.904	0.714	1.325	100.2
2	24.84	2.957	12.14	0.563	2.974	12.54	25.35	2.511	9.512	2.407	1.614	0.709	0.818	1.1	100
3	27.04	1.363	5.495	0.286	2.367	13.87	31.58	2.929	10.35	2.139	1.393	0.494	0.481	0.538	100.3
4	27.9	1.524	5.593	0.332	2.489	14.11	29.93	2.998	10.18	2.271	1.455	0.607	0.481	0.513	100.4
5	25.6	1.295	5.45	0.288	2.461	14.41	31.15	2.917	10.4	2.247	1.46	0.461	0.503	0.545	99.19
6	26.89	1.961	7.356	0.338	2.036	11.56	31.06	2.941	10.42	2.014	1.328	0.618	0.487	0.653	99.65
7	26.05	1.572	6.036	0.294	2.294	13.27	31.5	2.924	10.58	2.142	1.484	0.701	0.502	0.544	99.89
8	27.8	1.308	7.231	0.469	2.653	10.27	30.18	2.719	10.27	2.204	1.586	0.699	0.87	0.684	98.94
9	28.48	2.092	7.4	0.312	2.99	9.007	29.36	2.669	10.48	2.303	1.62	0.827	0.641	0.727	98.91
21-mon-02															
1	26.48	3.433	14.12	0.559	2.784	7.95	25.18	2.485	9.55	2.212	1.625	0.693	0.81	1.261	99.15
2	25.64	2.673	10.97	0.471	2.413	10.88	27.77	2.65	9.636	2.338	1.412	0.705	0.782	0.969	99.31
3	27.72	1.917	7.849	0.384	2.288	11.6	30.09	3.011	10.23	1.895	1.416	0.55	0.607	0.705	100.3
4	26.35	2.306	9.087	0.43	2.324	11.84	29.68	2.807	9.938	2.174	1.414	0.674	0.562	0.853	100.4
5	26.11	2.424	9.187	0.415	2.429	11.48	28.96	2.703	10.18	2.175	1.364	0.616	0.582	0.868	99.5
6	26.36	1.872	7.457	0.34	2.132	12.77	31.65	2.826	10.2	1.905	1.365	0.465	0.512	0.669	100.5
7	27.9	1.922	7.629	0.317	2.01	11.92	30.81	2.858	10.23	2.079	1.304	0.652	0.478	0.705	100.8
8	28.07	1.242	6.429	0.367	2.488	12.85	30.78	2.84	10.3	2.065	1.523	0.621	0.664	0.623	100.9
9	28.84	1.334	5.847	0.286	2.354	11.18	31.4	2.837	10.41	2.206	1.428	0.65	0.603	0.537	99.92
10	28.72	1.302	6.522	0.341	2.372	11.61	31.12	2.864	10.2	1.89	1.387	0.627	0.719	0.649	100.3
21-mon-03															
1	26.12	2.615	10.85	0.584	2.876	10.26	27.3	2.646	9.744	2.373	1.729	0.845	0.647	0.998	99.58
2	26.25	2.432	9.788	0.48	2.662	12.96	27.69	2.494	9.554	2.325	1.626	0.812	0.665	0.949	100.7
3	25.32	2.755	11.49	0.528	2.928	11.77	26.42	2.482	9.898	2.279	1.642	0.926	0.699	1.113	100.3
4	25.13	3.023	11.48	0.517	2.563	11.3	26.54	2.676	9.645	2.236	1.5	0.646	0.729	1.099	99.07
5	28.74	1.407	7.115	0.404	2.508	11.22	29.96	2.729	9.901	2.186	1.372	0.746	0.726	0.663	99.68
6	27.35	2.23	9.436	0.389	2.5	11.15	28.13	2.642	10.08	2.116	1.691	0.644	0.633	0.831	99.82
7	26.39	2.18	8.715	0.406	2.597	11.48	29.11	2.905	10.01	2.239	1.611	0.704	0.546	0.842	99.73
8	25.85	2.764	10.89	0.458	2.485	11.91	27.78	2.559	9.66	2.396	1.584	0.585	0.735	0.961	100.6
9	27.27	2.763	10.85	0.566	2.708	11.59	27.23	2.67	9.776	2.288	1.616	0.584	0.648	0.998	101.6
10	25.59	3.034	10.84	0.542	2.779	10.22	27.31	2.717	10.04	2.167	1.693	0.824	0.661	1.053	99.46

Table 4. Data from sample 21 from West Água Rasa metagranite. Monazite U-Th-Pb_T ages, U, Th and Pb contents and respective errors. MPb is the average Pb atomic mass.

West Água Rasa monazite from sample 21

	Age	Error	U	Error	Th	Error	Pb	Error	M Pb
	21-mon-01								
	Ma	**Ma**	**ppm**	**%**	**ppm**	**%**	**ppm**	**%**	**ppm**
1	1960	42	4305	2.3	118620	1.0	12300	1.0	207.7
2	1798	39	4284	2.3	106669	1.0	10211	1.0	207.7
3	1900	65	2214	4.5	48290	1.0	4994	2.0	207.7
4	1750	61	2614	3.8	49151	1.0	4762	2.1	207.7
5	1933	66	2234	4.5	47895	1.0	5059	2.0	207.7
6	1766	52	2568	3.9	64645	1.0	6062	1.6	207.7
7	1776	60	2254	4.4	53044	1.0	5050	2.0	207.7
8	1773	50	3730	2.7	63546	1.0	6350	1.6	207.6
9	1964	55	2336	4.3	65031	1.0	6749	1.5	207.8
	21-mon-02								
	Age	**Error**	**U**	**Error**	**Th**	**Error**	**Pb**	**Error**	**M Pb**
	Ma	Ma	ppm	%	ppm	%	ppm	%	ppm
1	1810	39	4138	2.4	124104	1.0	11706	1.0	207.8
2	1773	41	3538	2.8	96440	1.0	8995	1.1	207.8
3	1770	50	2946	3.4	68977	1.0	6545	1.5	207.7
4	1853	46	3282	3.0	79857	1.0	7918	1.3	207.7
5	1876	47	3144	3.2	80735	1.0	8058	1.2	207.7
6	1785	52	2580	3.9	65532	1.0	6210	1.6	207.7
7	1858	53	2368	4.2	67044	1.0	6545	1.5	207.8
8	1854	57	2875	3.5	56498	1.0	5783	1.7	207.7
9	1807	62	2194	4.6	51383	1.0	4985	2.0	207.7
10	1927	58	2641	3.8	57315	1.0	6025	1.7	207.7
	21-mon-03								
	Age	**Error**	**U**	**Error**	**Th**	**Error**	**Pb**	**Error**	**M Pb**
	Ma	**Ma**	**ppm**	**%**	**ppm**	**%**	**ppm**	**%**	**ppm**
1	1783	40	4541	2.2	95385	1.0	9264	1.1	207.7
2	1900	44	3684	2.7	86017	1.0	8810	1.1	207.7
3	1915	41	4012	2.5	100992	1.0	10332	1.0	207.7
4	1900	41	3915	2.6	100869	1.0	10202	1.0	207.7
5	1790	52	3163	3.2	62527	1.0	6155	1.6	207.7
6	1778	45	2901	3.4	82924	1.0	7714	1.3	207.8
7	1907	48	3091	3.2	76587	1.0	7816	1.3	207.7
8	1777	41	3428	2.9	95736	1.0	8921	1.1	207.8
9	1792	40	4382	2.3	95385	1.0	9264	1.1	207.7
10	1897	42	4171	2.4	95271	1.0	9775	1.0	207.7

5. DISCUSSION

To characterize the West Água Rasa metagranite there were correlated petrographic analyses and whole rock geochemical data from samples 18A, 18B, 19A, 19B, 21A, and 21B. Then the outcomes were associated with U-Th-Pb_T geochronology results of three monazite grains from sample 21A. The geochemical results, combined with the petrography, were used to classify the rock, its protolith, and genesis. With the geochemical data, it was possible to correlate the genesis with events already discussed in previous studies (Chaves and Rezende, 2019; Miranda et al., 2020).

From the texture and mineral assemblage observed in thin sections (Fig. 2 and Fig. 3), associated with TAS classification (Middlemost, 1994) (Fig. 3B), it was possible to confirm that the samples were metamonzogranites. The geochemical data classified the rock with peraluminous nature (Fig. 3B and C) and as S-type granite (Fig. 3E, F, and G), both indicating supracrustal origin. Moreover, the results indicated that the rock has metasedimentary origin (Fig. 4E), confirming that the protolith was formed on an oceanic basin, followed by anatexis of khondalitic graphite-rich rocks and banded iron formations. Finally, the granite genesis is associated to syn to post-collisional events (Fig. 4C and D). The anomalies of Eu and Sr (Fig. 4A and B) are related to the process of metasediments anatexis. They present different anomalies in samples 18A, 18B, 21A, and 21B (negative) and in samples 19A and 19B (positive) due to the predominance of plagioclase in the second group. The higher concentration of plagioclases in these samples can be explained either by the predominance of minerals rich in Ca in the metasediments that form the metagranites or as a product of a more advanced phase of the anatexis process.

The geochronological data yielded two groups of ages, as shown in Table 5. The Orosirian age is consistent with ages found by Miranda et al. (2020) in Água Rasa metagranites. Their results revealed ages of 2077 ± 24 Ma and 1941 ± 23 from monazite and 1934 ± 74 Ma from zircon U-Pb. They characterize the younger ages (~1940 Ma), that are concordant to the results from West Água Rasa metagranites, to the orogen collapse after post-peak decompressional stage, which are coherent to the geochemical results found in samples 21A and 21B (Fig. 4B).

Table 5. Monazite U-Th-Pb_T mean ages from sample 21, West Água Rasa metagranite.

	Age (Ma)	
Grain	**Orosirian**	**Statherian**
21-mon-01	1946 ± 27	1778 ± 22
21-mon-02	1871 ± 36	1789 ± 20
21-mon-03	1904 ± 19	1784 ± 19

The Statherian ages can be correlated with Avanavero-Xiong'er LIP, in which the Pará de Minas dyke swarm, that crosses the entire area of study (Fig. 1A), is part (Chaves and Rezende, 2019). This hydrothermal process, that occurred around 1.78 ~ 1.79 Ga, was responsible for a regional warming that affected the West Água Rasa metagranites, preserving this event in the monazite. The grains show corroded appearance (Fig. 5), typical of hydrothermal dissolution processes, which corroborates this analysis.

6. CONCLUSION

The West Água Rasa metagranite was formed from the anatexis of supracrustal succession rocks. The melting process occurred due to the decompression-related orogenic collapse of the Rhyacian-Orosirian event that occurred around 1.90 Ga. A regional warming, associated with the Avanavero-Xiong'er LIP, that is represented in the area by the Pará de Minas dykes swarm, happened between 1.78 and 1.79 Ga and affected the West Água Rasa metagranite. The influence is evidenced by the corroded appearance of monazite grains that presented Statherian age.

7. ACKNOWLEDGEMENTS

The first author acknowledges the Coordenação de Aperfeiçoamento de Pessoal de Nível Superior - Brasil (CAPES) for the research grant. The second author thanks the support of the Conselho Nacional de Desenvolvimento Científico e Tecnológico (CNPq).

8. REFERENCES

Alkmim F.F., Martins-Neto M.A., 2001. A Bacia Intracratônica do São Francisco: Arcabouço estrutural e cenários evolutivos. In: Martins-Neto M.A., Pinto C.P. (Eds.). Bacia do São Francisco. Belo Horizonte: SBG-MG, 9-30.

Ashworth, J.R., 1985. Migmatites. Blackie and Son, Glasgow. 302.

Ávila C.A., Teixeira W., Bongiolo E.M., Dussin I.A., Vieira T.A.T., 2014. Rhyacian evolution of subvolcanic and metasedimentary rocks of the southern segment of the Mineiro belt, São Francisco Craton, Brazil. Precambrian Research, 243, 221-251.

Baltazar O.F., Zucchetti M., 2007. Lithofacies associations and structural evolution of the Archean Rio das Velhas greenstone belt, Quadrilátero Ferrífero, Brazil: A review of the setting of gold deposits. Ore Geology Reviews, 32, 471-499.

Batchelor, R.A., Bowden, P., 1985. Petrogenetic interpretation of granitoid rock series using multicationic parameters. Chemical Geology, 48, 43-55.

Brown, M., Solar, G.S., 1998. Granite ascent and emplacement during contractional deformation in convergent orogens. Journal of Structural Geology, 20, 1365-1393.

Carneiro, M.A., Barbosa, M.S.C., 2008. Implicações geológicas e tectônicas da interpretação magnetométrica da região de Oliveira, Minas Gerais: Revista Brasileira de Geofísica, 26, 87–98.

Carvalho, B.B., Janasi, V.A., Sawyer, E.W., 2017. Evidence for Paleoproterozoic anatexis and crustal reworking of Archean crust in the São Francisco Craton, Brazil: a dating and isotopic study of the Kinawa migmatite. Precambrian Research, 291, 98-118.

Chaves, A.O., 2013. Enxames de diques máficos de Minas Gerais – O estado da arte: Geonomos, 21, 29–33.

Chaves, A.O., Oliveira, E.K., Garcia, L.R.A., 2013. Desenvolvimento do método de datação química U-Th-Pb de monazita por microssonda eletrônica na UFMG: Geonomos, 21, 13–18.

Chaves A.O., Campello M.S., Pedrosa-Soares A.C., 2015. Idade U-Th-PbT de monazitas do sillimanita-cordierita-granada-biotita gnaisse de Itapecerica (MG) e a atuação da orogenia Riaciano-Orosiriana no interior do Cráton São Francisco Meridional. Geociências, 34, 324-334.

Chaves, A.O., Rezende, C.R., 2019. Fragments of 1.79-1.75 Ga Large Igneous Provinces in reconstructing Columbia (Nuna): A Statherian supercontinent-superplume coupling?, Episodes, 24, 55–67.

Chaves, A.O., 2021. Columbia (Nuna) supercontinent with external subduction girdle and concentric accretionary, collisional and intracontinental orogens permeated by large igneous provinces and rifts. Precambrian Research, 352, 106017.

Chaves, A.O., Porcher, C.C., 2020. Petrology, geochemistry and Sm-Nd systematics of the Paleoproterozoic Itaguara retroeclogite from São Francisco/Congo Craton: one of the oldest records of the modern-style plate tectonics. Gondwana Research, 87, 224-237.

Chappell, B.W., White, A.J., 2001. Two contrasting granite types: 25 years later. Australian Journal of Earth Sciences, 48, 489-499.

CPRM/CODEMIG., 2014. Estado de Minas Gerais-Mapa Geológico e Mapa de Recursos Minerais em Sistema de Informação Geográfica/SIG. Escala 1: 1000000. Serviço Geológico do Brasil/CPRM e Companhia de Desenvolvimento Econômico de Minas Gerais/ CODEMIG. DVD Rom.

Dorr J.V.N., 1969. Physiographic, stratigraphic and structural development of the Quadrilatero Ferrifero, Minas Gerais, Brazil, U.S. Geological Survey Professional Paper, 641, 110.

Drummond, J.B., Pufahl, P.K., Porto, C.G., Carvalho, M., 2015. Neoproterozoic peritidal phosphorite from the Sete Lagoas Formation (Brazil) and the Precambrian phosphorus cycle. Sedimentology, 62, 1978-2008.

Edmonds, M., Gill, R., 2010. Igneous Rocks and Processes: A Practical Guide. Geological Magazine, 147, 990.

Farina F.A., Albert C., Lana C., 2015. The Neoarchean transition between medium and high-K granitoids: Clues from the Southern São Francisco Craton (Brazil). Precambrian Research, 266, 375-394.

Fernandes, R.A., Carneiro, M.A.O., 2000. Complexo Metamórfico Campo Belo (Craton São Francisco Meridional): Unidades litodêmicas e evolução tectônica: Revista Brasileira de Geociencias, 30, 671–678.

Frost, B. R., Barnes, C. G., Collins, W. J., Arculus, R. J., Ellis, D. J., Frost, C. D., 2001. A geochemical classification for granitic rocks. Journal of petrology, 42, 2033-2048.

Harris, N., Vance, D., Ayres, M., 2000. From sediment to granite: timescales of anatexis in the upper crust. Chemical Geology, 162, 155-167.

Laurent, O., Martin, H., Moyen, J. F., Doucelance, R., 2014. The diversity and evolution of late-Archean granitoids: Evidence for the onset of "modern-style" plate tectonics between 3.0 and 2.5 Ga. Lithos, 205, 208-235.

Ludwig, K.R., 2003. Isoplot/Ex 3.00: A geochronological toolkit for Microsoft Excel: Berkeley Geochronology Center, Special Publication, 4, 70.

Machado, N., Schrank, A., Noce, C.M., Gauthier, G., 1996. Ages of detrital zircon from Archean-Paleproterozoic sequences: Implications for greenstone belt setting and evolution of a Transamazonian foreland basin in Quadrilátero Ferrífero, southeast Brazil: Evidence from zircon ages by laser ablation ICP-MS. Earth Planetary Science Letters, 141, 259-276.

Machado Filho, L., Ribeiro, M., Gonzales, S.R., Schenini, C.A., Santos Neto, A., Palmeira, R.C., Pires, J.L., Teixeira, W., Castro, H.E.F., 1983. Geologia das folhas Rio de Janeiro (SF 23/24) escala 1:1.000.000, mapa e texto explicativo. Rio de Janeiro: RADAM Brasil, Ministério das Minas e Energia, 780.

Maniar, P.D., Piccoli, P.M., 1989. Tectonic discriminations of granitoids. Geological Socitey of America Bulletin, 101, 635–643.

Middlemost, E.A.K., 1994. Naming materials in magma/igneous rock system. Earth-Science Reviews, 37, 215–224.

Miranda, D.A., Chaves, A.D.O., Dussin, I.A., Porcher, C.C., 2020. Paleoproterozoic khondalites in Brazil: a case study of metamorphism and anatexis in khondalites from Itapecerica supracrustal succession of the southern São Francisco Craton. International Geology Review, 1-25.

Moreira, H., Lana, C., Nalini Júnior, H.A., 2016. The detrital zircon record of an Archaean convergent basin in the Southern São Francisco Craton, Brazil. Precambrian Research, 275, 84-99.

Noce, C.M., Machado, N., Teixeira, W., 1998. U-Pb Geochronology of gneisses and granitoids in the Quadrilatero Ferrıfero (Southern São Francisco Craton): Age constraints for

Archean and Paleoproterozoic magmatism and metamorphism. Revista Brasileira de Geociências, 28, 95-102.

Noce, C.M., Pedrosa-Soares, A.C., Silva, L.C.D., Alkmim, F.F., 2007. O embasamento arqueano e paleoproterozóico do orógeno Araçuaí. Geonomos, 15, 17-23.

Pearce, J., 1996. Sources and settings of granitic rocks. Episodes, 19, 120-125.

Pommier, A., Cocherie, A., Legendre, O., 2004. EPMA Dating User's manual: Age calculation from electron probe microanalyser measurements of U-Th-Pb. BRGM Documents, 9.

Read, H. H., 1943. Meditations on granite: part one. Proceedings of the Geologists' Association, 54, 64-85.

Streckeisen, A.L., 1974. Classification and Nomenclature of Plutonic Rocks: Recommendations of the IUGS Subcommission on the Systematics of Igneous Rocks. Geologische Rundschau. Internationale Zeitschrift für Geologie. Stuttgart, 63, 773–786.

Sun, S.S., McDonough, W.F., 1989. Chemical and isotopic systematics of oceanic basalts, implications for mantle composition and processes, in Saunders, A.D., Norry, M.J., eds., Magmatism in the ocean basins, Volume 42: London, Geological Society of London, 313–345.

Teixeira, W., Carneiro, M.A., Noce, C.M., Machado, N., Sato, K., Taylor, P.N., 1996. Pb, Sr and Nd isotope constraints on the Archean evolution of gneissic-granitoid complexes in the southern São Francisco Craton, Brazil. Precambrian Research, 78, 151-164.

Teixeira, W., Ávila, C.A., Dussin, I.A., Corrêa Neto, A.V., Bongiolo, E.M., Santos, J.O.S., Barbosa, N., 2015. A juvenile accretion episode (2.36–2.33 Ga) in the Mineiro belt and its role to the long-lived Minas accretionary orogeny: zircon U–Pb–Hf and geochemical evidences. Precambrian Research, 256, 148-169.

Teixeira, W., Oliveira, E.P., Peng, P., Dantas, E.L., Hollanda, M.H.B.M., 2017. U-Pb geochronology of the 2.0 Ga Itapecerica graphite-rich supracrustal succession in the São Francisco Craton: Tectonic matches with the North China Craton and paleogeographic inferences. Precambrian Research, 293, 91-111.

Toya, T., Kato, A., Jotaki, R., 1984. Quantitative Analysis with Electron Probe Microanalyzer. Jeol Training Center. Japan. 113.

Whalen, J.B., Currie, K.L., Chappell, B.W., 1987. A-type granites: geochemical characteristics, discrimination and petrogenesis. Contributions to mineralogy and petrology, 95, 407-419.

Whitney D.L., Evans B.W., 2010. Abbreviations for names of rock-forming minerals. American Mineralogist, 95,185-187.

Zhou, J., Li, X. 2006. GeoPlot: An excel VBA program for geochemical data plotting: Computers e Geosciences, 32, 554–560.

FINAL COMMENTS

The elliptical geophysical anomalies between the cities of Formiga and Itapecerica triggered the interest in studying the rocks in this area. The investigation on graphite schist and metagranite samples led to the tectonic evolution of the region. With the results it was possible to confirm the influence of the Rhyacian-Orosirian orogeny (Chaves et al. 2015; Teixeira et al. 2017) and the Avanavero-Xiong'er LIP event (Chaves, 2021) on southern São Francisco Craton.

The presence of todorokite, Mn-oxide mineral typical of deep-sea Mn nodules formed by microorganisms, in the graphite schist from Formiga-MG supports the biogenic origin proposed by Miranda et al. (2019) for kind of rock in Itapecerica-MG. The same authors found monazite U-Th-Pb_T age of 2090 ± 26 Ma, related to the metamorphic peak on 729ºC that occurred in the Paleoproterozoic orogeny in Itapecerica area. The results presented here, however, showed temperature around 460ºC. This temperature is associated with a hydrothermalism affecting graphite from Formiga that occurred in a post-collisional stage.

The West Água Rasa metagranite, that was collected in the edge of the anomalies, yielded ages around 1,90 Ga and 1,78 Ga. The Orosirian age is associated with the decompression-related orogenic collapse of the Rhyacian-Orosirian event, which lead to the melting process of the supracrustal succession (khondalitic graphite-rich rocks and banded iron formations) located in the interior of the anomalies, to generate the metagranites. Finally, the Statherian age is related to the regional warming promoted by the Avanavero-Xiong'er LIP, that is represented in the area by the Pará de Minas dykes swarm.

Fig. 3 shows a tectonic model modified from Carvalho et al. (2017) and Miranda et al. (2019) for the formation of the Formiga graphite-rich rocks and metagranite in Paleoproterozoic. During the pre-collisional stage (2.35–2.08 Ga) the CM-rich sedimentary sequence was deposited on an oceanic basin. Such sequence was involved during the collision stage (2.07–2.01 Ga) and the biogenic carbonaceous material (CM) transformed into graphite under high-grade metamorphism. Finally, at the post-collisional stage (~1.90 Ga) there was the collapse of the previously formed orogen accompanied by metagranite formation and intense hydrothermal activity affecting graphite. This tectonic model is part of a huge collisional orogenic process concentrically developed along all Columbia (Nuna), as shown in Fig. 4 (Chaves, 2021). Black square shows the location of the investigated Formiga Paleoproterozoic processes in Fig. 4.

Lastly, the Avanavero-Xiong'er LIP (Fig. 5) event (Chaves, 2021) was responsible for affecting the monazite grains that yielded Statherian ages on U-Th-Pb geochronological

analyses, due to hydrothermal activity triggered by this event, which could have also contributed to lowering temperature found in graphite from Formiga.

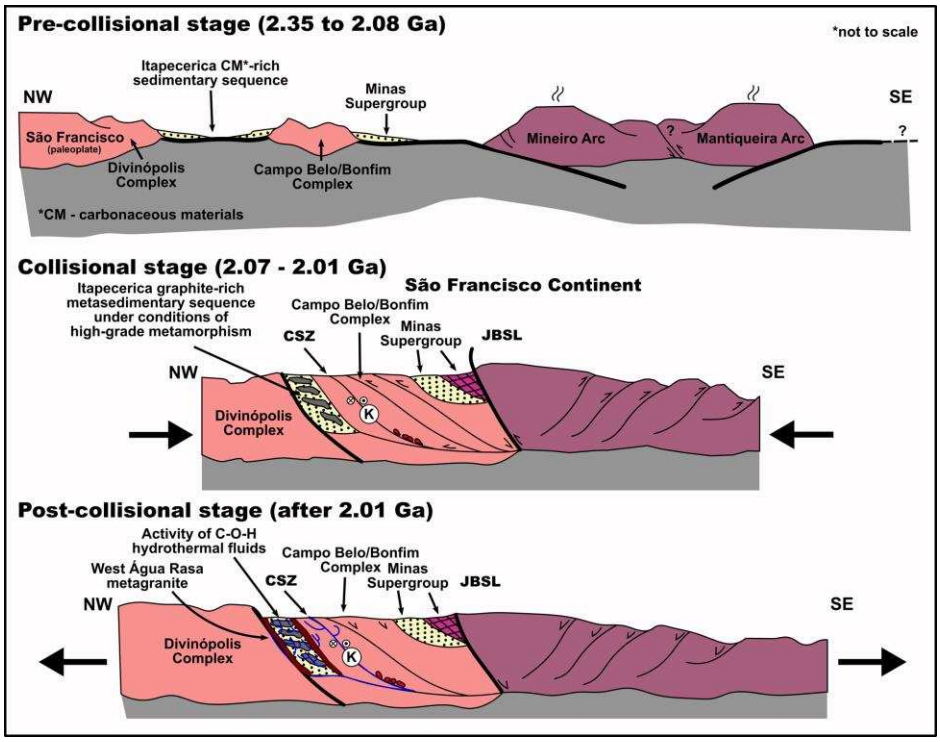

Fig. 3 - Illustration (adapted from Carvalho et al. 2017) of a tectonic model for the formation of the graphite from Formiga. K: Kinawa migmatite; CSZ: Claudio Shear Zone; JBSL: Jeceaba-Bom Sucesso lineament.

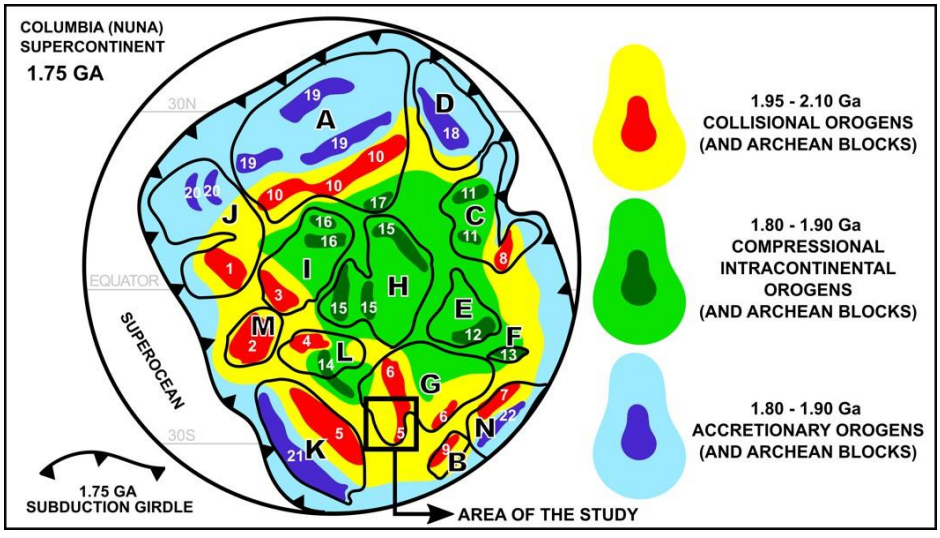

Fig. 4 - Distribution of concentric collisional (1.95–2.10 Ga), accretionary and compressional intracontinental (1.80–1.90 Ga) orogens and undiscriminating Archean blocks on 1.75 Ga Columbia (Nuna) reconstruction. Modified from Chaves (2021). A – Laurentia; B – Kalahari; C – Australia; D – Mawson/East Antarctica; E – India; F – Tarim; G – São Francisco/Congo; H – Siberia; I – West Africa; J – Baltica; K - Amazonia; L – North China; M – Rio de La Plata; N – Tanzania; 1 – Volga-Don/Baltica; 2 – Tandilia-Piedra Alta/Rio de la Plata; 3 – Birimian/West Africa; 4 – Khondalite Belt/North China; 5 – Transamazonian/Amazonia and São Francisco craton; 6 – Eburnean and Luizian/Congo craton; 7 – Usagaran/Tanzania; 8 – Glenburg/West Australia; 9 – Limpopo/Kalahari; 10 – Taltson-Thelon and Inglefield/Laurentia; 11 – Mount Isa and Halls Creek/North Australia; 12 – Lesser Himalaya/India; 13 – Tarim/Tarim; 14 – Transnorth China/North China; 15 – Angara, Akitkan, and Sutam/Siberia; 16 – Zenaga and Reguibat/West Africa; 17 – Wopmay/Laurentia; 18 – Nimrod-Ross/East Antarctica; 19 – Trans Hudson, Torngat-Quebec, and Nagssugtoqidian/Laurentia; 20 – Lapland and Svecofennian/Baltica; 21 – Rio Negro-Juruena/Amazonia; 22 – Ubendian/Tanzania.

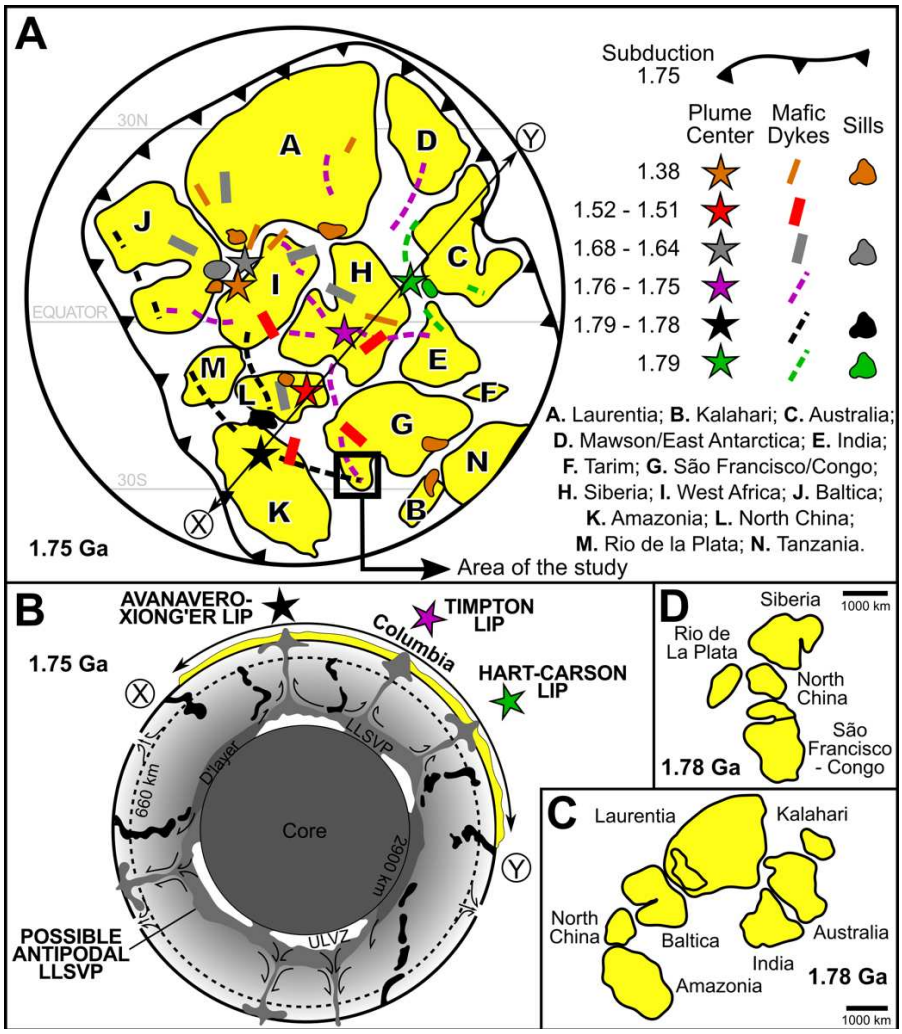

Fig. 5 - (A) 1.75 Ga Columbia (Nuna) reconstruction model derived from matching Paleo- to Mesoproterozoic LIP fragments on different cratonic pieces. Radiating dyke systems (and associated volcanics and sills) of not only 1.79 Ga, 1.79–1.78 Ga, and 1.76–1.75 Ga, but also 1.64–1.68 Ga, 1.51–1.52 Ga, and 1.38 Ga LIPs restored on the Columbia (Nuna) are shown with their respective possible plume centers. (B) Supercontinent-superplume coupling suggested for Columbia (Nuna). LLSVP = large low shear velocity provinces, ULVZ = ultra-low velocity zones, SUPERPLUME = cluster of mantle plumes starting from a LLSVP. Modified from Chaves (2021). (C) 1.78 Ga positioning of the India, Australia, Laurentia, Baltica, North China and Amazonia blocks after Pesonen et al. (2012). (D) Statherian positioning of the North China, Rio de la Plata, São Francisco/Congo and Siberia blocks after Xu et al. (2017).

REFERENCES

Alkmim, F.F., Martins-Neto, M.A., 2001. A Bacia Intracratônica do São Francisco: Arcabouço estrutural e cenários evolutivos. In: Martins-Neto M.A., Pinto C.P. (Eds.). Bacia do São Francisco. Belo Horizonte: SBG-MG, p.9-30.

Almeida, F.F.M., Hasui, Y., Brito-Neves, B.B., Fuck, R.A., 1997. As províncias estruturais do Brasil. In: SBG, Simpósio de Geologia do Nordeste, 8, Bol. Esp., p.12.

Ávila, C.A., Teixeira, W., Bongiolo, E.M., Dussin, I.A., Vieira, T.A.T., 2014. Rhyacian evolution of subvolcanic and metasedimentary rocks of the southern segment of the Mineiro belt, São Francisco Craton, Brazil. Precambrian Research, v. 243, p. 221–251.

Baltazar, O.F. & Zucchetti, M., 2007. Lithofacies associations and structural evolution of the Archean Rio das Velhas greenstone belt, Quadrilátero Ferrífero, Brazil: A review of the setting of gold deposits. Ore Geology Reviews, v.32(3-4), p.471-499.

Campello, M.S., Vaz, B.B., Oliveira, M.A.S., Ávila, M.A.C., 2015. Relatório e mapa geológicos 1:100.000 da Folha Formiga SF.23-V-B-III. Projeto Fortaleza de Minas, CODEMIG/UFMG. A.C. Pedrosa Soares (coord.). p.62.

Carvalho, B.B., Janasi, V.A., Sawyer, E.W., 2017. Evidence for Paleoproterozoic anatexis and crustal reworking of Archean crust in the São Francisco Craton, Brazil: A dating and isotopic study of the Kinawa migmatite. Precambrian Research, v.291, p.98–118.

Chaves, A.O., 2013. Enxames de diques máficos de Minas Gerais – O estado da arte: Geonomos, v.21, p.29–33.

Chaves, A.O., Campello, M.S., Pedrosa-Soares, A.C., 2015. Idade U-Th-PbT de monazitas do sillimanita-cordierita-granada-biotita gnaisse de Itapecerica (MG) e a atuação da orogenia Riaciano-Orosiriana no interior do Cráton São Francisco Meridional. Geociências, v.34, p.324-334.

Chaves, A.O., Porcher, C.C., 2020. Petrology, geochemistry and Sm-Nd systematics of the Paleoproterozoic Itaguara retroeclogite from São Francisco/Congo Craton: one of the oldest records of the modern-style plate tectonics. Gondwana Research, v.87, p.224-237.

Chaves, A.O., 2021. Columbia (Nuna) supercontinent with external subduction girdle and concentric accretionary, collisional and intracontinental orogens permeated by large igneous provinces and rifts. Precambrian Research, 352, 106017.

CPRM/CODEMIG., 2014. Estado de Minas Gerais-Mapa Geológico e Mapa de Recursos Minerais em Sistema de Informação Geográfica/SIG. Escala 1: 1000000. Serviço

Geológico do Brasil/CPRM e Companhia de Desenvolvimento Econômico de Minas Gerais/ CODEMIG. DVD Rom.

Dorr, J.V.N., 1969. Physiographic, stratigraphic and structural development of the Quadrilatero Ferrifero, Minas Gerais, Brazil, U.S. Geological Survey Professional Paper, 641-A, p.110.

Drummond, J.B., Pufahl, P.K., Porto, C.G., Carvalho, M., 2015. Neoproterozoic peritidal phosphorite from the Sete Lagoas Formation (Brazil) and the Precambrian phosphorus cycle. Sedimentology, v.62, p.1978-2008.

Farina, F.A., Albert, C., Lana, C. 2015. The Neoarchean transition between medium and high-K granitoids: Clues from the Southern São Francisco Craton (Brazil). Precambrian Research, v.266, p.375–394.

Machado Filho, L., Ribeiro, M., Gonzales, S.R., Schenini, C.A., Santos Neto, A., Palmeira, R.C., Pires, J.L., Teixeira, W., Castro, H.E.F., 1983. Geologia das folhas Rio de Janeiro (SF 23/24) escala 1:1.000.000, mapa e texto explicativo. Rio de Janeiro: RADAM Brasil, Ministério das Minas e Energia, p.780.

Miranda, D.A., Chaves, A.O., Campello, M.S., Ramos, S.L.L.M., 2019. Origin and thermometry of graphites from Itapecerica supracrustal succession of the southern Sao Francisco Craton by C isotopes, X-ray diffraction, and Raman spectroscopy. International Geology Review.

Miranda, D.A., Chaves, A.D.O., Dussin, I.A., Porcher, C.C., 2020. Paleoproterozoic khondalites in Brazil: a case study of metamorphism and anatexis in khondalites from Itapecerica supracrustal succession of the southern São Francisco Craton. International Geology Review, 1-25.

Moreira, H., Lana, C., Nalini Júnior, H.A., 2016. The detrital zircon record of an Archaean convergent basin in the Southern São Francisco Craton, Brazil. Precambrian Research, v.275, p.84-99.

Noce, C.M., Machado, N., Teixeira, W., 1998. U-Pb Geochronology of gneisses and granitoids in the Quadrilatero Ferrıfero (Southern São Francisco Craton): Age constraints for Archean and Paleoproterozoic magmatism and metamorphism. Revista Brasileira de Geociências, v.28, p.95-102.

Noce, C.M., Pedrosa-Soares, A.C., Silva, L.C.D., Alkmim, F.F.O., 2007. embasamento arqueano e paleoproterozóico do orógeno Araçuaí. Geonomos, v.15, p.17-23.

Ruy, A.C., Silva, A.M., Toledo, C.L.B., Souza Filho, C.R., 2006. Uso de dados aerogeofísicos de alta densidade para mapeamento geológico em terrenos altamente intemperizados:

O estudo de caso da região de Cláudio, porção sul do Cráton São Francisco: Revista Brasileira de Geofísica, v.24, n.4, p.535–546.

Teixeira, W., Carneiro, M.A., Noce, C.M., Machado, N., Sato, K., Taylor, P.N., 1996. Pb, Sr and Nd isotope constraints on the Archean evolution of gneissic-granitoid complexes in the southern São Francisco Craton, Brazil. Precambrian Research, v.78, p.151-164.

Teixeira, W., Ávila, C.A., Dussin, I.A., Corrêa Neto, A.V., Bongiolo, E.M., Santos, J.O.S., Barbosa, N., 2015. A juvenile accretion episode (2.36–2.33 Ga) in the Mineiro belt and its role to the long-lived Minas accretionary orogeny: zircon U–Pb–Hf and geochemical evidences. Precambrian Research, v.256, p.148-169.

Teixeira, W., Oliveira, E.P., Peng, P., Dantas, E.L., Hollanda, M.H.B.M., 2017. U-Pb geochronology of the 2.0 Ga Itapecerica graphite-rich supracrustal succession in the São Francisco Craton: Tectonic matches with the North China Craton and paleogeographic inferences. Precambrian Research, v.293, p.91-111.